Core Surveillance of Boiling-Water Reactors

Zwisler Jensen, L.

Publication date:
1981

Document Version
Publisher's PDF, also known as Version of record

RISØ

Risø-R-445

Core Surveillance of Boiling-Water Reactors

Lars Zwisler Jensen

Risø National Laboratory, DK-4000 Roskilde, Denmark
September 1981

RISØ-R-445

CORE SURVEILLANCE OF BOILING-WATER REACTORS

Lars Zwisler Jensen

Abstract. Methods suitable for a calculational procedure which determines the three-dimensional power distribution in boiling-water reactors on the basis of in-core detector readings are described. A two-dimensional equation based on diffusion theory is set up, and a method for incorporating detector readings in the solution of this equation is presented. A three-dimensional calculational method based on nodal theory is developed. Calculations are carried out using this method, and the results are compared with a three-dimensional nodal theory calculation. Finally, parameters affecting the detector readings are examined.

INIS-discriptors. BWR TYPE REACTORS; IN-CORE INSTRUMENTS; MATHEMATICAL MODELS; MONITORING; NEUTRON DETECTORS; POWER DISTRIBUTION; REACTOR CORES; THREE-DIMENSIONAL CALCULATIONS; TWO-DIMENSIONAL CALCULATIONS.

UDC 621.039.51:621.039.524-97

September 1981

Risø National Laboratory, DK-4000 Roskilde, Denmark

ISBN 87-550-0793-7
ISSN 0106-2840

Risø Repro 1984

CONTENTS

1. INTRODUCTION

Light-water reactors are provided with detectors by means of which the power distribution can be measured. However, for economic and practical reasons the number of detectors is limited and the power distribution can be determined at only a limited number of points in the reactor. Therefore, a calculational procedure is required which determines the three-dimensional power distribution on the basis of the detector readings. Methods that may be used for such a procedure are developed in this report. Special reference is made to boiling-water reactors because of accessibility of data for this type of reactor. First, the detector system of a boiling-water reactor is described. Most boiling-water reactors are equipped with both fixed and axially movable in-core detectors, and for such reactors correlations between readings and power values have been applied. The correlations use precalculated fitting constants. An alternative to the correlation method is presented next. A two-dimensional equation based on diffusion theory is set up, and a method for incorporating detector readings in the solution of this equation is described. A similar procedure is developed based on nodal theory, and a three-dimensional calculational method is worked out using this procedure and a one-dimensional nodal theory calculation together with correlation factors. Finally, parameters affecting the detector readings are examined.

2. THE CORRELATION METHOD

2.1. Boiling-water reactor in-core instrumentation

Boiling-water reactors are monitored by means of a monitoring system consisting of fixed and traversing in-core detectors[1,2]. The instrument tube accomodating both fixed and movable detectors is located in a water gap at the corner of four adjacent fuel assemblies. The fixed detectors are positioned axially at four equally spaced locations. There is approximately one instrument tube for every sixteen fuel assemblies. The arrangement of detectors in a horizontal plane is such that when all the detector locations are rotated into one quadrant, all interior fuel assemblies in that quadrant are adjacent to a detector.

The fixed and traversing in-core detectors both contain miniature fission chambers which measure the local neutron flux. The fixed detectors are calibrated using the traversing ones. One instrument tube location near the center of the core can be reached by each traversing in-core detector so that each of these detectors can be normalized to a common value. The power distribution is determined by means of the fixed in-core detectors using stored traversing in-core detector readings to get values for axial levels where no fixed in-core detectors are located. A condition for using stored readings of the traversing in-core detectors is that no significant change in the control rod setting has taken place since the measurements were made. If the control rod setting has changed or sufficient time has elapsed, a new run will be made with the traversing in-core detectors.

2.2. The correlation method

The box power is inferred from the detector readings using correlation factors[3]. The first step in this calculation is to find the average power in the four fuel rods immediately surrounding the detector. The correlation used is derived from two-dimensional box calculations and depends on the four-box average exposure and void fraction. The correlation is independent of adjacent control rod positions. It has the following form

$$\begin{aligned} PAR(L,K) = (&CAR_1 + CAR_2 \cdot E + CAR_3 \cdot E^2 + CAR_5 \cdot EV \\ &+ CAR_6 \cdot E^2V + CAR_7 \cdot EV^2 + CAR_8 \cdot V \\ &+ CAR_9 \cdot V^2 + CAR_{10} \cdot V^3) \cdot ER(L,K) \end{aligned} \qquad (2.2.1)$$

where

- L = identification of radial detector location
- K = identification of axial detector location
- PAR(L,K) = four adjacent rod average power at radial position L and axial position K
- ER(L,K) = detector reading at radial position L and axial position K
- E = average void fraction in four adjacent fuel segments
- CAR_i = correlation factor i = 1,10

The next step in the power distribution calculation is to find the average power of the four fuel segments surrounding the detector at each specified elevation, given the four rod average power at that position. The correlation derived from the two-dimensional box calculations involves a coupled void fraction-control rod pattern and a separable exposure-dependent factor as follows:

$$P4B(L,K) = \frac{PAR(L,K)}{FL(I)\cdot(1-FV(I)\cdot V)(1+PE_1\cdot E+PE_2\cdot E^2+PE_3\cdot E^3)} \qquad (2.2.2)$$

where

P4B(L,K) = four-box average power at position L,K
PAR(L,K) = four adjacent rod power at position L,K
E = four-segment average exposure
V = four-segment average void fraction
PE_i = correlation constants i = 1, 3
FL(I) = control rod pattern and configuration type dependent factor
FV(I) = control rod pattern and configuration type dependent void multiplier

Finally the power in an individual fuel box segment is given by

$$P(L,J,K) = P4B(L,K) \cdot PAL(L,J,K) \qquad (2.2.3)$$

where

P(L,J,K) = fuel segment power at position L,J,K

The power allocation factor PAL(L,J,K) is separated into the following factors:

$$\begin{aligned} PAL\ (L,J,K) = {} & RPM(M(L,J,K)) \\ & \cdot (1 + CVM(M) \cdot (VP(L,J,K) - V4B(L,K))) \\ & \cdot (1 + CEM(EXP(L,J,K) - E4B(L,K))) \\ & \cdot CTM(lTYP, IT) \cdot GR(L,J,K) \end{aligned} \qquad (2.2.4)$$

where

M(L,J,K) = control rod pattern and orientation with respect to segment L,J,K
RPM(M) = control rod pattern-dependent power mismatch factor
V4B(L,K) = average void fraction at position L,K

VF(L,J,K) = void fraction in segment L,J,K
CVM(M) = rod pattern-dependent void fraction power mismatch factor
E4B(L,K) = average four-box fuel exposure at L,K
EXF(L,J,K) = fuel exposure of segment L,J,K
CEM = constant coefficient in exposure mismatch factor
ITYP = type of fuel box in position L,J
CTM(ITYP,IT) = box and configuration type-dependent power mismatch factor
GR(L,J,K) = gross gradient-dependent power mismatch factor

The gross gradient power mismatch correction GR(L,J,K) for each fuel box is a weighting factor obtained by fitting a polynomial to the three reading in a diagonal line intersecting the given box, interpolating to the position of the box and normalizing with respect to the central reading.

Given the fuel segment power the peak rod power is determined using a local peaking factor which is predetermined from a two-dimensional box calculation. The local peaking factor is a function of fuel segment exposure and void fraction, control rod position, and fuel and configuration type and may be expressed

$$FLOP(L,J,K) = FPK(M,ITYP,IT) \cdot (1+APK(1,TYP) \cdot E+APK(2,ITYP) \cdot E^2) \cdot (1+APK(3 \text{ or } 5,ITYP) \cdot V+APK(4 \text{ or } 6,ITYP) \cdot V^2) \qquad (2.2.5)$$

where

E + EXF(L,J,K) = fuel segment exposure
V = VF(L,J,K) = fuel segment void fraction
FRP(M,ITYP,IT) = control rod pattern and fuel and configuration type-dependent factor of local peaking factor
APK(i,ITYP) = correlation constants,i = 1,6

The coefficients of V and V^2 are taken to be APK_3 and APK_4, respectively, if fuel segment L,J,K has the adjacent control rod inserted, but are taken to be APK_5 and APK_6 if the fuel segment is uncontrolled. The maximum rod power density in segment L,J,K is then given by

$$MRPD(L,J,K) = \frac{P(L,J,K) \cdot FLOP(L,J,K)}{NRB(ITYP)\ Z_s} (1-FLK-FCH) \qquad (2.2.6)$$

where

NRB (ITYP) = number of rods per box of fuel type ITYP
Z_s = fuel segment length
FLK = fraction of core power deposited in the leakage region
FCH = fraction of core power deposited in the active channel flow by nonconvection mechanisms

The peak heat flux $Q_{PK}(L,J,K)$ in fuel segment (L,J,K) is similarly determined

$$Q_{PK}\ (L,J,K) = \frac{P(L,J,K) \cdot FLOP(L,J,K) \cdot C1 \cdot (1-FLK-FCH)}{AHT(ITYP)\ Z_s} \qquad (2.2.7)$$

where AHT(ITYP) is the fuel heat transfer area per unit length per box.

The critical heat flux (CHF) is determined from a (mass-velocity, pressure- and quality-dependent) heat flux correlation and the critical heat flux ratio is defined as

$$CHFR = CHF/PHF \qquad (2.2.8)$$

where PHF is the peak heat flux.

3. ACCELERATED DIFFUSION THEORY

3.1. Henry's method for coarse mesh calculations

The two-group equations for fast and thermal flux are

$$-\underline{\nabla}\cdot D_1\underline{\nabla}\phi_1+\Sigma_{R1}\phi_1 = \frac{1}{\lambda}(\nu\Sigma_{f1}\phi_1+\nu\Sigma_{f2}\phi_2) \qquad (3.1.1)$$

$$-\underline{\nabla}\cdot D_2\underline{\nabla}\phi_2+\Sigma_{a2}\phi_2 = \Sigma_{s12}\phi_1 \qquad (3.1.2)$$

where

D_1 = fast diffusion constant
Σ_{R1} = removal cross section
λ = eigenvalue
$\nu\Sigma_{f1}$ = fast production cross section
$\nu\Sigma_{f2}$ = thermal production cross section
D_2 = thermal diffusion constant
Σ_{a2} = thermal absorption cross section
Σ_{s12} = slowing-down cross section
Σ_{a1} = fast absorption cross section
ϕ_1 = fast flux
ϕ_2 = thermal flux

Σ_{R1}, Σ_{a1} and Σ_{s12} are related by

$$\Sigma_{R1} = \Sigma_{a1} + \Sigma_{s12} \qquad (3.1.3)$$

Modified one-group theory can be derived from the two-group equations in the following way: It is assumed that thermal leakage is negligible in comparison with thermal absorption, i.e.

$$-\nabla\cdot D_2\nabla\phi_2 \ll \Sigma_{a2}\phi_2 \qquad (3.1.4)$$

If the thermal buckling is B^2, the above condition is

$$D_2 B^2/\Sigma_{a2} << 1 \tag{3.1.5}$$

The equation for the thermal flux then reduces to

$$\Sigma_{a2} \phi_2 = \Sigma_{s12} \phi_1 \tag{3.1.6}$$

Thus the thermal flux is proportional to the fast flux

$$\phi_2 = \frac{\Sigma_{s12}}{\Sigma_{a2}} \phi_1 \tag{3.1.7}$$

When this expression for the thermal flux is inserted in the equation for the fast flux, one has

$$-\underline{\nabla} \cdot D_1 \underline{\nabla} \phi_1 + \Sigma_{R1} \phi_1 = \frac{1}{\lambda} (\nu\Sigma_{f1} \phi_1 + \frac{\Sigma_{s12}}{\Sigma_{a2}} \nu\Sigma_{f2} \phi_1) \tag{3.1.8}$$

Taking $\Sigma_{R1} \phi_1$ outside the parenthesis on the right-hand side of the equation, one has

$$-\underline{\nabla} \cdot D_1 \underline{\nabla} \phi_1 + \Sigma_{R1} \phi_1 = \frac{1}{\lambda} (\frac{\nu\Sigma_{f1}}{\Sigma_{R1}} + \frac{\Sigma_{s12}}{\Sigma_{a2}} \frac{\nu\Sigma_{f2}}{\Sigma_{R1}}) \Sigma_{R1} \phi_1 \tag{3.1.9}$$

If the nuclear parameters are renamed in the following way

$$\Sigma_1 = \Sigma_{R1} \tag{3.1.10}$$

$$k_\infty = \frac{\nu\Sigma_{f1}}{\Sigma_{R1}} + \frac{\Sigma_{s12}}{\Sigma_{R1}} \frac{\nu\Sigma_{f2}}{\Sigma_{a2}} \tag{3.1.11}$$

the equation for the fast flux is formally identical to the one-group equation

$$-\underline{\nabla}\cdot D_1 \underline{\nabla}\phi_1 + \Sigma_1\phi_1 = \frac{1}{\lambda} k_\infty \Sigma_1\phi_1 \qquad (3.1.12)$$

This method is referred to as 1½ group theory 4).

For D_1 independent of space

$$-\nabla \cdot D_1 \nabla \phi_1 = -D_1 \nabla^2 \phi_1 \qquad (3.1.13)$$

and

$$\nabla^2\phi_1 + \frac{\frac{k_\infty}{\lambda} - 1}{D_1} \Sigma_1\phi_1 = 0 \qquad (3.1.14)$$

Consider a reactor subdivided into nodes of uniform material properties. For the two-dimensional case a node will be characterized by subscripts i and j, the node lying between the cartesian coordinates x_i and x_{i+1} and y_j and y_{j+1}. Quantities associated with the node will be labelled ij and the mesh interval in the x and y directions will be named h_i and h_j, respectively.

The one-group equation for this case takes the form

$$\nabla^2 \phi_1 + B_{ij}^2 \phi_1 = 0 \qquad (3.1.15)$$

where

$$B_{ij}^2 = \frac{\frac{k_{\infty ij}}{\lambda} - 1}{D_{1ij}} \Sigma_{1ij} \qquad (3.1.16)$$

The following definitions are introduced

$$J_{x,i,j} = -D_{ij} \frac{\partial}{\partial x} \int_{y_j}^{y_{j+1}} \frac{1}{h_j} \phi(x_i,y)dy \qquad (3.1.17)$$

$$J_{y,i,j} = -D_{ij} \frac{\partial}{\partial y} \int_{x_i}^{x_{i+1}} \frac{1}{h_i} \phi(x,y_j)dx \qquad (3.1.18)$$

$$\phi_j(x) = \int_{y_j}^{y_{j+1}} \frac{1}{h_j} \phi(x,y)dy \qquad (3.1.19)$$

$$\phi_i(y) = \int_{x_i}^{x_{i+1}} \frac{1}{h_i} \phi(x,y)dy \qquad (3.1.20)$$

$$B_y^2(x) = -1/\phi_j(x) \int_{y_j}^{y_{j+1}} \frac{1}{h_j} \frac{\partial^2}{\partial y^2} \phi\,(x,y)dy \qquad (3.1.21)$$

$$B_x^2(y) = -1/\phi_i(y) \int_{x_i}^{x_{i+1}} \frac{1}{h_i} \frac{\partial^2}{\partial x^2} \phi\,(x,y)dx \qquad (3.1.22)$$

The left-hand side of the equation is integrated over the interval from y_j to y_{j+1}

$$\frac{1}{h_j} \int_{y_j}^{y_{j+1}} \left(\frac{\partial^2\phi}{\partial x^2} + \frac{\partial^2\phi}{\partial y^2} + B^2\phi\right) dy$$

$$= \frac{\partial^2}{\partial x^2} \int_{y_j}^{y_{j+1}} \frac{1}{h_j} \phi(x,y)\, dy + \int_{y_j}^{y_{j+1}} \frac{1}{h_j} \frac{\partial^2}{\partial y^2} \phi(x,y)\, dy$$

$$+ B^2 \int_{y_j}^{y_{j+1}} \frac{1}{h_j} \phi(x,y)\, dy$$

$$= \frac{\partial^2}{\partial x^2} \phi_j(x) - B_y^2(x)\, \phi_j(x) + B^2\, \phi_j(x) \qquad (3.1.23)$$

Thus $\phi_j(x)$ satisfies the following equation

$$\frac{\partial^2\phi_j}{\partial x^2} + (B^2 - B_y{}^2(x)\phi_j(x) = 0 \qquad (3.1.24)$$

Integration of the left-hand side of this equation over the interval from x_i to x_{i+1} gives

$$\int_{x_i}^{x_{i+1}} \frac{\partial^2 \phi_j}{\partial x^2}\, dx + \int_{x_i}^{x_{i+1}} (B^2 - B_y^2(x))\, \phi_j(x)\, dx = 0 \qquad (3.1.25)$$

The first integral is simply

$$\int_{x_i}^{x_{i+1}} \frac{\partial^2 \phi_j}{\partial x^2}\, dx = \frac{\partial}{\partial x}\, \phi_j(x_{i+1}) - \frac{\partial}{\partial x}\, \phi_j(x_i)$$

$$= -1/D_{ij}\, (J_{x,i+1,j} - J_{x,i,j}) \qquad (3.1.26)$$

The second integral is split into two parts, the first of which is

$$\int_{x_i}^{x_{i+1}} B^2\, \phi_j(x)dx = h_i \frac{1}{h_i h_j} \int_{x_i}^{x_{i+1}} \int_{y_j}^{y_{j+1}} B^2\, \phi(x,y)dx\, dy = h_i\, \phi_{i,j} B^2 \qquad (3.1.27)$$

where $\phi_{i,j}$ is the average flux of node ij.

Thus

$$\int_{x_i}^{x_{i+1}} -B_y^2(x)\, \phi_j(x)dx + h_i\, \phi_{i,j}\, B^2 - 1/D_{ij}(J_{x,i+1,j} - J_{x,i,j}) = 0 \qquad (3.1.28)$$

Now, integrating the one-group equation over node ij one has

$$\iint (\nabla^2 \phi + B^2 \phi)dxdy = \iint \underline{\nabla} \cdot (-\frac{1}{D_{ij}}\, \underline{J})dxdy + B^2 h_i h_j \phi_{i,j} \qquad (3.1.29)$$

$\iint \nabla \cdot J\, dxdy$ may be evaluated using Gauss's theorem

$$\iint \underline{\nabla} \cdot \underline{J}\, dx\, dy = \int_c \underline{J} \cdot \underline{n}\, ds \qquad (3.1.30)$$

where the circulation is taken around the circumference of the node and n is an outward normal. Furthermore

$$\int_c \underline{J} \cdot \underline{n}\, ds = \int_{x_i}^{x_{i+1}} -J_y(x,y_j)dx + \int_{y_j}^{y_{j+1}} J_x(x_{i+1},y)dy + \int_{x_{i+1}}^{x_i} J_y(x,y_{j+1}) \cdot (-dx) + \int_{y_{j+1}}^{y_j} -J_x(x_i,y)(-dy)$$

$$= -h_i J_{y,i,j} + h_j J_{x,i+1,j} + h_i J_{y,i,j+1} - h_j J_{x,i,j}$$

$$= h_i(J_{y,i,j+1} - J_{y,i,j}) + h_j(J_{x,i+1,j} - J_{x,i,j}) \qquad (3.1.31)$$

$$\iint (\nabla^2 \phi + B^2 \phi)dxdy = -\frac{1}{D_{ij}} \iint \underline{\nabla} \cdot \underline{J}\, dxdy + B^2 h_i h_j \phi_{i,j}$$

$$= -\frac{1}{D_{ij}} h_i(J_{y,i,j+1} - J_{y,i,j}) - \frac{1}{D_{ij}} h_j(J_{x,i+1,j} - J_{x,i,j}) + B^2 h_i h_j \phi_{i,j}$$

$$= 0 \qquad (3.1.32)$$

$\phi_{i,j}$ is determined by

$$B^2 \phi_{i,j} = \frac{1}{D_{ij}h_j}(J_{y,i,j+1} - J_{y,i,j}) + \frac{1}{D_{ij}h_i}(J_{x,i+1,j} - J_{x,i,j}) \qquad (3.1.33)$$

Finally

$$\int_{x_i}^{x_{i+1}} B_y^2(x)\, \phi_j(x)dx = h_i\, \phi_{i,j}\, B^2 - \frac{1}{D_{ij}}(J_{x,i+1,j} - J_{x,i,j})$$

$$= h_i/h_j(J_{y,i,j+1} - J_{y,i,j}) \qquad (3.1.34)$$

The transverse bucklings B_y^2 and B_x^2 are defined by

$$B_y^2 = 1/\phi_{i,j} \int_{x_i}^{x_{i+1}} 1/h_i\, B_y^2(x)\, \phi_j(x)dx \qquad (3.1.35)$$

$$B_x^2 = 1/\phi_{i,j} \int_{y_j}^{y_{j+1}} 1/h_j\, B_x^2(y)\, \phi_i(y)dy \qquad (3.1.36)$$

and the above equation becomes

$$B_y^2 = \frac{J_{y,i,j+1} - J_{y,i,j}}{D_{ij}\phi_{ij}\, h_j} \qquad (3.1.37)$$

The corresponding equation for the x-direction becomes

$$B_x^2 = \frac{J_{x,i+1,j} - J_{x,i,j}}{D_{ij}\phi_{ij}\, h_i} \qquad (3.1.38)$$

Accordingly one has

$$B_x^2 + B_y^2 = B^2 \qquad (3.1.39)$$

$B_y^2(x)$ and $B_x^2(y)$ will be approximated in this way

$$B_y^2(x) \equiv B_y^2 \qquad 3.1.40)$$

$$B_x^2(y) \equiv B_x^2 \qquad 3.1.41)$$

The equation

$$\frac{\partial^2}{\partial x^2}\ \phi_j(x) + (B^2 - B_y^2(x))\ \phi_j(x) = 0 \qquad (3.1.42)$$

reduces to

$$\frac{\partial^2}{\partial x^2}\ \phi_j(x) + B_x^2\ \phi_j(x) = 0 \qquad (3.1.43)$$

$\phi j(x)$ being a function of x alone, this is an ordinary differential equation with constant coefficients, which can be solved analytically.

Similarly, the equation

$$\frac{\partial^2}{\partial y^2}\ \phi_i(y) + (B^2 - B_x^2(y))\ \phi_i(y) = 0 \qquad (3.1.44)$$

reduces to

$$\frac{\partial^2}{\partial y^2}\,\phi_i(y) + B_y^2\,\phi_i(y) = 0 \qquad (3.1.45)$$

Now consider two neighbouring nodes (i+1,j) and (i,j). The differential equation to be solved is in node (i,j)

$$\frac{\partial^2 \phi_j}{\partial x^2} + B_{x,i,j}^2\,\phi_j(x) = 0 \qquad (3.1.46)$$

and in node (i+1,j)

$$\frac{\partial^2 \phi_j}{\partial x^2} + B_{x,i+1,j}\,\phi_j(x) = 0 \qquad (3.1.47)$$

For node (i,j) the general solution is

$$\phi_j(x) = A_{i,j}\,\sin(B_{x,i,j}\,x) + C_{i,j}\,\cos(B_{x,i,j}\,x) \qquad (3.1.48)$$

The average flux in node (i,j) is

$$\phi_{i,j} = \frac{1}{h_i}\int_{x_i}^{x_{i+1}} \phi_j(x)dx$$

$$= \frac{1 - \cos(B_{x,i,j}\,h_i)}{h_i\,B_{x,i,j}}\,A_{i,j} + \frac{\sin(B_{x,i,j}\,h_i)}{h_i\,B_{x,i,j}}\,C_{i,j} \qquad (3.1.49)$$

The average current $J_{x,i+1,j}$ is

$$J_{x,i+1,j} = -\,D_{i,j}\,\frac{\partial}{\partial x}\,\phi_j(x)\Big|_{x=h_i}$$

$$= -\,D_{i,j}\,B_{x,i,j}\,A_{i,j}\,\cos(B_{x,i,j}\,h_i)$$

$$+\,D_{i,j}\,B_{x,i,j}\,C_{i,j}\,\sin(B_{x,i,j}\,h_i) \qquad (3.1.50)$$

We now have two equations in the unknowns $A_{i,j}$ and $C_{i,j}$.

Solving the equations for these we have

$$A_{i,j} = B_{x,i,j}\, h_i\, \phi_{i,j} - 1/(D_{i,j}\, B_{x,i,j})\, J_{x,i+1,j} \qquad (3.1.51)$$

$$C_{i,j} = \frac{1}{D_{ij}\, B_{x,i,j}} \cdot \frac{1 - \cos(B_{x,i,j}\, h_i)}{\sin(B_{x,i,j}\, h_i)}\, J_{x,i+1,j}$$

$$+ \frac{B_{x,i,j}\, h_i}{\sin(B_{x,i,j}\, h_i)} \cdot \cos(B_{x,i,j}\, h_i)\, \phi_{ij} \qquad (3.1.52)$$

For node (i+1,j) the solution is written

$$\phi_{\,j}(x) = A_{i+1,j} \sin B_{x,i+1,j}(x - x_{i+1})$$

$$+ C_{i+1,j} \cos B_{x,i+1,j}(x - x_{i+1}) \qquad (3.1.53)$$

The average flux is

$$\phi_{i+1,j} = \frac{1 - \cos(B_{x,i+1,j}\, h_{i+1})}{h_{i+1}\ B_{x,i+1,j}}\, A_{i+1,j}$$

$$+ \frac{\sin(B_{x,i+1,j}\, h_{i+1})}{h_{i+1}\, B_{x,i+1,j}}\, C_{i+1,j} \qquad (3.1.54)$$

The average current $J_{x,i+1,j}$ is

$$J_{x,i+1,j} = - D_{i+1,j}\, B_{x,i+1,j}\, A_{i+1,j} \qquad (3.1.55)$$

Solving these two equations for $A_{i+1,j}$ and $C_{i+1,j}$, one gets

$$A_{i+1,j} = - 1/(D_{i+1,j}\, B_{x,i+1,j})\, J_{x,i+1,j} \qquad (3.1.56)$$

$$C_{i+1,j} = \frac{h_{i+1}}{D_{i+1,j}} \frac{1 - \cos(B_{x,i+1,j}\, h_{i+1})}{B_{i+1,j}\, h_{i+1} \sin(B_{x,i+1,j}\, h_{i+1}} J_{x,i+1,j}$$

$$+ \frac{h_{i+1}\, B_{x,i+1,j}}{\sin(B_{x,i+1,j}\, h_{i+1})}\, \phi_{i+1,j} \qquad (3.1.57)$$

Continuity of flux and current at the interface applies to average flux and current as well.

Continuity of the average flux at the interface infers that

$$C_{i+1,j} = A_{i,j} \sin(B_{x,i,j}\, h_i) + C_{i,j} \cos(B_{x,i,j}\, h_i) \quad (3.1.58)$$

Using the expressions for $C_{i+1,j}$, $A_{i,j}$ and $C_{i,j}$, one gets

$$\frac{h_{i+1}}{D_{i+1,j}} \frac{1 - \cos(B_{x,i+1,j}\, h_{i+1})}{B_{x,i+1,j}\, h_{i+1} \sin(B_{x,i+1,j}\, h_{i+1})} J_{x,i+1,j}$$

$$+ \frac{h_{i+1}\, B_{x,i+1,j}}{\sin(B_{x,i+1,j} h_{i+1})} \phi_{i+1,j}$$

$$= (B_{x,i,j}\, h_i\, \phi_{i,j} - J_{x,i,j}/(D_{i,j}\, B_{x,i,j})) \sin(B_{x,i,j}\, h_i)$$

$$+ \frac{1}{D_{ij}\, B_{x,i,j}} \frac{1 - \cos(B_{x,i,j}\, h_i)}{\sin(B_{x,i,j}\, h_i)} J_{x,i,j}$$

$$+ \frac{B_{x,i,j}\, h_i}{\sin(B_{x,i,j}\, h_i)} \cos(B_{x,i,j}\, h_i) \quad (3.1.59)$$

From this equation, $J_{x,i+1,j}$ may be expressed in terms of $\phi_{i,j}$ and $\phi_{i+1,j}$

$$J_{x,i+1,j} = \frac{\dfrac{B_{x,i,j}\, h_i}{\sin(B_{x,i,j}\, h_i)} \phi_{i,j} - \dfrac{B_{x,i+1,j}\, h_{i+1}}{\sin(B_{x,i+1,j}\, h_{i+1})} \phi_{i+1,j}}{\dfrac{h_i}{D_{i,j}} \dfrac{1 - \cos(B_{x,i,j}\, h_i)}{B_{x,i,j} h_i \sin(B_{x,i,j} h_i)} + \dfrac{h_{i+1}}{D_{i+1,j}} \dfrac{1 - \cos(B_{x,i+1,j}\, h_{i+1})}{B_{x,i+1,j} h_{i+1} \sin(B_{x,i+1,j} h_{i+1})}} \quad (3.1.60)$$

3.2. Linearization of Hanry's Method

It is assumed that the terms $B_{x,i,j}\ h_i$ are small compared with unity

$$B_{x,i,j}\ h_i \ll 1 \tag{3.2.1}$$

As a consequence, the following relations are valid to the first order in $B_{x,i,j}^2\ h_i^2$ 5,6)

$$\frac{B_{x,i,j}\ h_i}{\sin\ (B_{x,i,j}\ h_i)} = \frac{B_{x,i,j}\ h_i}{B_{x,i,j}\ h_i - 1/6\ B_{x,i,j}^3\ h_i^3}$$

$$= \frac{1}{1 - 1/6\ B_{x,i,j}^2\ h_i^2}$$

$$= 1 + 1/6\ B_{x,i,j}^2\ h_i^2 \tag{3.2.2}$$

$$\frac{1 - \cos(B_{x,i,j}\ h_i)}{B_{x,i,j}\ h_i \sin\ (B_{x,i,j}\ h_i)}$$

$$= \frac{1-(1-1/2\ B_{x,i,j}^2\ h_i^2+1/24\ B_{x,i,j}^4 h_i^4)}{B_{x,i,j}h_i(B_{x,i,j}h_i - 1/6\ B_{x,i,j}^3 h_i^3)}$$

$$= 1/2\ \frac{1 - 1/12\ B_{x,i,j}^2 h_i^2}{1 - 1/6\ B_{x,i,j}^2 h_i^2}$$

$$= 1/2\ (1 - 1/12\ B_{x,i,j}^2 h_i^2)(1 + 1/6\ B_{x,i,j}^2\ h_i^2)$$

$$= 1/2\ (1 + 1/12\ B_{x,i,j}^2\ h_i^2) \tag{3.2.3}$$

Insertion of these expansions in the equation relating $J_{x,i+1,j}$ to ϕ_{ij} and $\phi_{i+1,j}$ leads to

$$J_{x,i+1,j}$$

$$= \frac{(1 + 1/6\ B_{x,i,j}^2\ h_i^2)\ \phi_{i,j} - (1 + 1/6\ B_{x,i+1,j}^2\ h_{i+1}^2)\ \phi_{i+1,j}}{\frac{h_i}{2D_{i,j}}(1+1/12\ B_{x,i,j}^2\ h_i^2) + \frac{h_{i+1}}{2D_{i+1,j}}(1+1/12\ B_{x,i+1,j}^2\ h_{i+1}^2)} \qquad (3.2.4)$$

From now on we will write $h_i = h$. The right-hand side of the above equation is simplified further

$$J_{x,i+1,j} = \frac{(1+1/6\ B_{x,i,j}^2\ h^2)\phi_{i,j} - (1+1/6\ B_{x,i+1,j}^2\ h^2)\phi_{i+1,j}}{\frac{h}{2D_{i,j}} + \frac{h}{2D_{i+1,j}}}$$

$$\cdot\ 1/(1+1/12(1/D_{i,j}+1/D_{i+1,j})^{-1}(B_{x,i,j}^2\ h^2/D_{i,j}+B_{x,i+1,j}^2\ h^2/D_{i+1,j}))$$

$$= \frac{(1+1/6\ B_{x,i,j}^2\ h^2)\phi_{i,j} - (1+1/6\ B_{x,i+1,j}^2\ h^2)\phi_{i+1,j}}{\frac{h}{2D_{i,j}} + \frac{h}{2D_{i+1,j}}}$$

$$+\ 1/12\ (1/D_{i,j} + 1/D_{i+1,j})^{-2}\ 2/h$$

$$\cdot\ (-B_{x,i,j}^2\ h^2/D_{i,j}\ \phi_{i,j} + B_{x,i+1,j}^2\ h^2/D_{i+1,j}\ \phi\ i+1,j$$

$$-\ B_{x,i+1,j}^2\ h^2/D_{i+1,j}\ \phi_{i,j} + B_{x,i,j}^2\ h^2/D_{i,j}\ \phi\ i+1,j) \qquad (3.2.5)$$

The terms $B_{x,i+1,j}^2\ h^2\ \phi\ i,j$ and $B_{x,i,j}^2\ h^2\ \phi_{i+1,j}$ are rewritten in the following way

$$B_{x,i+1,j}^2\ h^2\ \phi_{i,j} = B_{x,i+1,j}^2\ h^2\ \phi\ i+1,j$$

$$+ (\phi_{i,j} - \phi_{i+1,j})\ B_{x,i+1,j}^2\ h^2 \qquad (3.2.6)$$

$$B_{x,i,j}^2 h^2 \phi_{i+1,j} = B_{x,i,j}^2 h^2 \phi_{i,j}^2 + (\phi_{i+1,j} - \phi_{i,j}) B_{x,i,j}^2 h^2 \quad (3.2.7)$$

Insertion in the expression for $J_{x,i+1,j}$ gives

$$J_{x,i+1,j} = \frac{(1+1/6\ B_{x,i,j}^2 h^2)\phi_{i,j} - (1+1/6\ B_{x,i+1,j}^2 h^2)\phi_{i+1,j}}{\frac{h}{2 D_{i,j}} + \frac{h}{2 D_{i+1,j}}}$$

$$+ 1/6\ 1/h(1/D_{i,j}+1/D_{i+1,j})^{-2}(B_{x,i+1,j}^2 h^2/D_{i+1,j}+B_{x,i,j}^2 h^2/D_{i,j}) \cdot (\phi_{i+1,j} - \phi_{i,j}) \quad (3.2.8)$$

The expression for $J_{x,i+1,j}$ is linearized neglecting the last term

$$J_{x,i+1,j} \approx \frac{(1+1/6\ B_{x,i,j}^2)\phi_{i,j} - (1+1/6\ B_{x,i+1,j}^2 h^2)\phi_{i+1,j}}{\frac{h}{2D_{i,j}} + \frac{h}{2D_{i+1,j}}} \quad (3.2.9)$$

However,

$$B_{x,i,j}^2 h^2 \phi_{i,j} = h/D_{i,j}(J_{x,i+1,j} - J_{x,i,j}) \quad (3.2.10)$$

$$B_{x,i+1,j}^2 h^2 \phi_{i+1,j} = h/D_{i+1,j}(J_{x,i+2,j} - J_{x,i+1,j}) \quad (3.2.11)$$

and so

$$B_{x,i,j}^2 h^2 \phi_{i,j} - B_{x,i+1,j}^2 h^2 \phi_{i+1,j} = h(1/D_{i,j} +1/D_{i+1,j})J_{x,i+1,j} - h/D_{i,j}\ J_{x,i,j} - h/D_{i+1,j}\ J_{x,i+1,j} \quad (3.2.12)$$

Rearranging terms, the expression for $J_{x,i+1,j}$ becomes

$$J_{x,i+1,j} = (1/D_{i,j} + 1/D_{i+1,j})^{-1}$$

$$\cdot(3/h(\phi_{i,j} - \phi_{i+1,j}) - J_{x,i,j}/2\ D_{i,j} - J_{x,i+2,j}/2D_{i+1,j}) \quad (3.2.13)$$

Similarly, the average current in the y-direction becomes

$$J_{y,i,j+1} = (1/D_{i,j} + 1/D_{i,j+1})^{-1}$$

$$\cdot\ (3/h(\phi_{i,j} - \phi_{i,j+1}) - J_{y,i,j}/2\ D_{i,j} - J_{y,i,j+2}/2\ D_{i,j+1})$$

(3.2.14)

In order to relate $J_{x,i,j+1}$ to average fluxes, the average currents $J_{x,i,j}$ and $J_{x,i+2,j}$ must be eleminated. This may be done by omitting the terms $B_{x,i,j}^{\ 2}\ h^2$ from the expression for $J_{x,i+1,j}$, yielding

$$J_{x,i+1,j} =$$

$$\frac{\phi_{i,j} - \phi_{i+1,j}}{\frac{h}{2D_{i,j}} + \frac{h}{2D_{i+1,j}}} = (1/D_{i,j} + 1/D_{i+1,j})^{-1}\ 2/h(\phi_{i,j} - \phi_{i+1,j}) \quad (3.2.15)$$

Applying this formula to the average currents $J_{x,i,j}$ and $J_{x,i+2,j}$, one gets

$$J_{x,i,j} = 2/h(1/D_{i-1,j} + 1/D_{i,j})^{-1}(\phi_{i-1,j} - \phi_{i,j}) \quad (3.2.16)$$

$$J_{x,i+2,j} = 2/h(1/D_{i+1,j} + 1/D_{i+2,j})^{-1}\ (\phi_{i+1,j} - \phi_{i+2,j})$$

(3.2.17)

The expression for $J_{x,i+1,j}$ becomes

$$J_{x,i+1,j} = (1/D_{i,j} + 1/D_{i+1,j})^{-1}$$

$$\cdot (3/h(\phi_{i,j} - \phi_{i+1,j})$$

$$- 1/D_{i,j}(1/D_{i-1,j} + 1/D_{i,j})^{-1}\, 1/h(\phi_{i-1,j} - \phi_{i,j})$$

$$- 1/D_{i+1,j}(1/D_{i+1,j} + 1/D_{i+2,j})^{-1}\, 1/h(\phi_{i+1,j} - \phi_{i+2,j}))$$

$$= 1/h(1/D_{i,j} + 1/D_{i+1,j})^{-1}$$

$$\cdot (\phi_{i,j}(3 + 1/D_{i,j}(1/D_{i-1,j} + 1/D_{i,j})^{-1})$$

$$- \phi_{i+1,j}(3 + 1/D_{i+1,j}(1/D_{i+1,j} + 1/D_{i+2,j})^{-1})$$

$$- \phi_{i-1,j}\, 1/D_{i,j}(1/D_{i-1,j} + 1/D_{i,j})^{-1}$$

$$+ \phi_{i+2,j}\, 1/D_{i+1,j}(1/D_{i+1,j} + 1/D_{i+2,j})^{-1}) \qquad (3.2.18)$$

If $D_{i-1,j} \approx D_{i,j}$, one has

$$1/D_{i,j}(1/D_{i-1,j} + 1/D_{i,j})^{-1} \approx 1/2 \qquad (3.2.19)$$

$$1/D_{i+1,j}(1/D_{i+1,j} + 1/D_{i+2,j})^{-1} \approx 1/2 \qquad (3.2.20)$$

and the expression for $J_{x,i+1,j}$ reduces to

$$J_{x,i+1,j} = 1/h(1/D_{i,j} + 1/D_{i+1,j})^{-1}$$

$$\cdot (7/2\ \phi_{i,j} - 7/2\ \phi_{i+1,j} - 1/2\ \phi_{i-1,j}$$

$$+ 1/2\ \phi_{i+2,j}) \qquad (3.2.21)$$

The one-group equation is

$$- \nabla \cdot D_1 \nabla \phi_1 + \Sigma_1 \phi_1 = 1/\lambda\ \kappa_\infty\ \Sigma_1 \phi_1 \qquad (3.2.22)$$

Since

$$J = -D_1 \nabla \phi_1$$

$$\nabla \cdot J + \Sigma_1 \phi_1 = 1/\lambda \kappa_\infty \Sigma_1 \phi_1 \qquad (3.2.23)$$

Integrating over a node and applying Gauss's theorem the neutron balance equation for a node results

$$h(J_{y,i,j+1} - J_{y,i,j} + J_{x,i+1,j} - J_{x,i,j}) + h^2 \Sigma_{1i,j}$$

$$= 1/\lambda \kappa_{\infty i,j} \Sigma_{1i,j} \phi_{i,j} h^2 \qquad (3.2.24)$$

The neutron balance equation states that the absorption and leakage of neutrons in a node must equal their production. Putting

$$AA1 = (1/D_{i,j} + 1/D_{i+1,j})^{-1} \qquad (3.2.25)$$

$$AA2 = (1/D_{i,j} + 1/D_{i-1,j})^{-1} \qquad (3.2.26)$$

$$AA3 = (1/D_{i,j} + 1/D_{i,j+1})^{-1} \qquad (3.2.27)$$

$$AA4 = (1/D_{i,j} + 1/D_{i,j-1})^{-1} \qquad (3.2.28)$$

and inserting the expression for the average currents in the neutron balance equation one gets

$$\phi_{i,j}(7/2(AA1 + AA2 + AA3 + AA4) + h^2 \Sigma_{1i,j})$$

$$+ \phi_{i-1,j}(- 1/2\ AA1 - 7/2\ AA2)$$

$$+ \phi_{i-2,j}\ 1/2\ AA2$$

$$+ \phi_{i+1,j}(- 1/2\ AA2 - 7/2\ AA1)$$

$$+ \phi_{i+2,j} \cdot 1/2\ AA1$$

$$+ \phi_{i,j-1}\ (- 1/2\ AA3 - 7/2\ AA4)$$

$$+ \phi_{i,j-2}\ 1/2\ AA4$$

$$+ \phi_{i,j+1}\ (-\ 7/2\ AA3 - 1/2\ AA4)$$

$$+ \phi_{i,j+2}\ 1/2\ AA3$$

$$= 1/\lambda\ \kappa_{\infty i,j}\ \Sigma_{1i,j}\ \phi_{i,j}\ h^2 \qquad (3.2.29)$$

3.3. Acceleration by means of detector readings

When the nodal balance equation is set up for all nodes in the reactor, a linear system of equations is obtained. The system has the form

$$A\ \phi = 1/\lambda\ B\ \phi \qquad (3.3.1)$$

The symbols have the following meaning:

A is a matrix describing absorption and leakage,
B is a matrix describing production,
ϕ is a vector of average fluxes, and
λ is an eigenvalue.

The equation is solved using an iterative method, where guesses are made at the eigenvalue λ and fluxvector ϕ and a new eigenvalue and fluxvector are estimated. If the method is properly chosen, the fluxvector and eigenvalue will converge after a smaller or greater number of iterations. When detectors are present in the core, the average power density at the location of the detectors may be measured. This can be used for accelerating convergence[6]). Since a detector is associated with the four fuel boxes surrounding it, the reactor will be grouped in cells of four boxes, some of which are instrumented and some of which are not. Only the two-dimensional case is treated in the sequel.

Let p be the power of an instrumented cell. Then the fluxes of an instrumented cell have to satisfy

$$E_o \sum_{\text{cell}} \phi_{i,j} \kappa\Sigma_{i,j} \Sigma_{li,j}/\nu = p \qquad (3.3.2)$$

E_o denotes the energy released per fission, and ν the number of neutrons produced per fission.

Solution of the linear system will in general render fluxes in the instrumented cells that do not satisfy this condition. Therefore, the problem is modified by introducing a diagonal matrix Ξ with 1's placed as diagonal elements for boxes belonging to cells without instrumentation, and ζ as diagonal elements for boxes in instrumented cells, ζ varying from cell to cell but having the same value for all boxes in a cell. The modified problem is

$$(A_D - 1/\lambda\ B)\ \Xi^{-1}\phi = (A_L + A_U)\phi \qquad (3.3.3)$$

$$C\ \phi = P \qquad (3.3.4)$$

The symbols have the following meaning

ϕ is a vector of fluxes arranged such that fluxes of the same cell follow consecutively,
A_D is a block diagonal matrix,
A_L is a lower triangular block matrix,
A_U is an upper triangular block matrix,
C is a matrix relating fluxes of instrumented cells to detector readings, and
p is a vector of detector readings.

A_D, A_L, and A_U are derived from the matrix A using

$$A = A_D - A_L - A_U \qquad (3.3.5)$$

Let the number of nodes be N and the number of detector locations be D. Then (3.3.3-4) constitutes a system of N+D equations. The unknowns of these equations are the fluxes, the number of which is N, and the elements of Ξ different from 1, the number of which is D; altogether there are N+D unknowns. Thus the number of equations equals the number of unknowns, and the problem is properly posed.

(3.3.3-4) is solved iteratively in the following way: First λ is set equal to unity and the flux distribution is assumed to be flat, i.e. all the elements of the flux vector ϕ are assumed to be 1. If a neutron balance equation of the form previously shown is applied, each cell is coupled to only the four surrounding cells. Now, consider a reactor in which the cells are ordered from left to right and from bottom to top with a cell characterized by subscripts (LX,LY). Then the flux vector of a cell $\phi_{LX,LY}$ consisting of four elements satisfies the following equations

$$(A_{D,LX,LY} - 1/\lambda\ B_{LX,LY})\ \Xi^{-1}_{LX,LY}\ \phi_{LX,LY}$$

$$= A_{L1,LX,LY}\ \phi_{LX-1,LY} + A_{L2,LX,LY}\ \phi_{LX,LY-1}$$

$$+ A_{U1,LX,LY}\ \phi_{LX,LY+1} + A_{U2,LX,LY}\ \phi_{LX+1,LY}$$

$$C_{LX,LY}\ \phi_{LX,LY} = P_{LX,LY} \qquad (3.3.6)$$

A_{L1} and A_{L2} are derived from A_L and A_{U1} and A_{U2} from A_U. The subscripts LX,LY after a matrix indicate the part of the matrix relevant to cell LX,LY.

Here

$$\Xi^{-1}_{LX,LY}\ \phi_{LX,LY} = 1/\zeta_{LX,LY}\ \phi_{LX,LY} \qquad (3.3.7)$$

Putting

$$\psi_{LX,LY} = 1/\zeta_{LX,LY}\ \phi_{LX,LY} \qquad (3.3.8)$$

the equations are solved cell by cell, from left to right and bottom to top. During the iteration number i, the fluxes of iteration i-1 are used to evaluate $\phi_{LX+1,LY}$ and $\phi_{LX,LY+1}$, whereas the fluxes of the iteration i have already been calculated for cell (LX-1,LY) and (LX,LY-1) and may be used to evaluate $\phi_{LX,-1,LY}$ and $\phi_{LX,LY-1}$.

First

$$(A_{D,LX,LY} - 1/\lambda\ B_{LX,LY})\ \psi^i_{LX,LY} =$$

$$A_{L1,LX,LY}\ \phi^i_{LX-1,LY} + A_{L2,LX,LY}\ \phi^i_{LX,LY-1}$$

$$+ A_{U1,LX,LY}\ \phi^{i-1}_{LX,LY+1} + A_{U2,LX,LY}\ \phi^{i-1}_{LX+1,LY} \qquad (3.3.9)$$

is solved for $\psi^i_{LX,LY}$. Since the matrices involved are of order 4 x 4, this is easily done.

Next

$$\zeta^i_{LX,LY}\ C_{LX,LY}\ \psi^i_{LX,LY} = P_{LX,LY} \qquad (3.3.10)$$

is solved for $\zeta^i_{LX,LY}$,

and finally $\phi^i_{LX,LY}$ is found using

$$\phi^i_{LX,LY} = \zeta^i_{LX,LY}\ \psi^i_{LX,LY}$$

The calculation continues by applying this procedure to the next cell. When all cells have been treated and the fluxvector ϕ^i has been found, the eigenvalue λ is adjusted. From the equation,

$$(A_D - 1/\lambda\ B)\ \Xi^{-1}\ \phi = (A_L + A_U)\ \phi \qquad (3.3.11)$$

a new estimate of λ can be derived operating on both sides by a transposed vector E^T of unit entries. This renders the following value,

$$\lambda_{i+1} = \frac{E^T B \Xi^{-1} \phi_i}{E^T(-A_L - A_U + A_D \Xi^{-1})\phi_i} \qquad (3.3.12)$$

A new fluxvector ϕ_{i+1} is determined based on the eigenvalue estimate λ_{i+1}, and this procedure is repeated until λ as well as ϕ do not change appreciably. Using EPS-1 and EPS-2 the iterations are stopped when ϕ_i and λ_i satisfy the convergence criteria

$$||\phi_i - \phi_{i-1}||/||\phi_i|| < \text{EPS-1} \qquad (3.3.13)$$

$$|\lambda_i - \lambda_{i-1}|/|\lambda_i| < \text{EPS-2} \qquad (3.3.14)$$

The fluxes in cell (LX,LY) are given numbers from 1 to 4 starting in the upper left corner of the cell and increasing when going clockwise round the cell. Consider box 1 in this cell. Using the neutron balance equation the elements of A_D, A_{L1}, A_{L2}, A_{U1}, A_{U2}, and B pertaining to this box are found to be

for A_D:

$$A_{D,11} = 7/2(AA1 + AA2 + AA3 + AA4) + h^2 \Sigma_{1i,j} \qquad (3.3.15)$$

$$A_{D,12} = -1/2\ AA2 - 7/2\ AA1 \qquad (3.3.16)$$

$$A_{D,13} = 0 \qquad (3.3.17)$$

$$A_{D,14} = -1/2\ AA3 - 7/2\ AA4 \qquad (3.3.18)$$

for A_{L1}:

$$A_{L1,11} = -\ 1/2\ AA2 \qquad (3.3.19)$$

$$A_{L1,12} = 1/2\ AA1 + 7/2\ AA2 \qquad (3.3.20)$$

$$A_{L1,13} = 0 \qquad (3.3.21)$$

$$A_{L1,14} = 0 \qquad (3.3.22)$$

for A_{U1}:

$$A_{U1,11} = -1/2\ AA3 \tag{3.3.23}$$

$$A_{U1,12} = 0 \tag{3.3.24}$$

$$A_{U1,13} = 0 \tag{3.3.25}$$

$$A_{U1,14} = 7/2\ AA3 + 1/2\ AA4 \tag{3.3.26}$$

for A_{U2}:

$$A_{U2,11} = -1/2\ AA1 \tag{3.3.27}$$

$$A_{U2,12} = 0 \tag{3.3.28}$$

$$A_{U2,13} = 0 \tag{3.3.29}$$

$$A_{U2,14} = 0 \tag{3.3.30}$$

for B:

$$B_{11} = \kappa_{\infty,i,j}\ \Sigma_{1,i,j}\ h^2 \tag{3.3.31}$$

$$B_{1j} = 0 \text{ for } j \neq 1 \tag{3.3.32}$$

The elements pertaining to other boxes are found similarly.

3.4. Test calculation

The method described has been applied to the test problem of Fig 3.4.1. The problem consists of an arrangement of boxes of two fuel types A and B, between some of which a control rod is inserted. A box of fuel type A with the adjacent control rod inserted is denoted A+, and similarly a box of fuel type B with an inserted control rod is denoted B+. At the boundaries zero current conditions are assumed. The arrangement is symmetrical about the diagonal. The two-group cross sections of the fuel

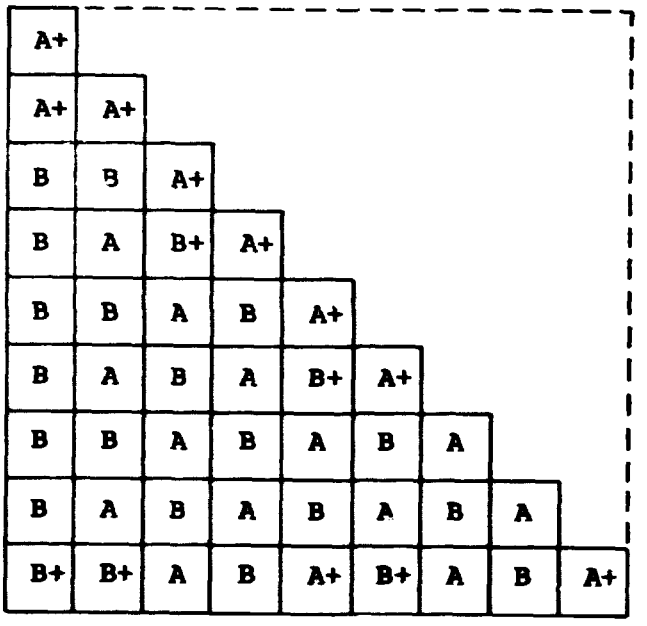

Fig. 3.4.1. Test problem. A and B are different fuel types; A+ and B+ are the same fuel types with a control rod inserted.

		A	A+	B	B+
D_1	cm	1.848200	1.872200	1.848200	1.872200
Σ_1	cm^{-1}	0.024817	0.025760	0.024818	0.025760
Σ_r	cm^{-1}	0.018744	0.017722	0.018744	0.017724
$\nu\Sigma_{f1}$	cm^{-1}	0.004555	0.004565	0.003795	0.003804
D_2	cm	0.465130	0.470180	0.465130	0.470170
Σ_2	cm	0.595400	0.074494	0.059538	0.074479
$\nu\Sigma_{f2}$	cm^{-1}	0.072652	0.075738	0.066051	0.068849

Fig. 3.4.2. Two-group cross sections for test problem.

types with and without a control rod inserted are given in Fig. 3.4.2. The test problem and the standard diffusion theory solution to it are given in reference 6.

Four configurations of detectors have been investigated: one with all cells monitored, one with half the cells monitored, one with a quarter of them monitored, and one with no detectors at all. The power distribution has been determined for all configurations and compared to the standard diffusion theory solution. A dot is used to symbolize a detector, and the average power of the cell provided by the standard diffusion theory solution is used as a detector reading. The results together with the percental errors are given in Fig. 3.4.3-6. The standard deviations of the estimated power distribution and the number of iterations required for convergence are given below for the four configurations.

Fraction of cells monitored	1.00	0.50	0.25	0.00
Standard deviation (%)	1.3	1.4	1.6	1.6
Number of iterations	6	7	14	41

Thus increasing the fraction of cells monitored reduces the number of iterations required for convergence and the standard deviation of the estimated power. The latter, however, had a small change. The impact on the standard deviation is believed to be greater when true detector readings are used instead of simulated readings such as those used here. The eigenvalue in all four cases was considered 0.995.

1. FIGURE : REFERENCE POWER
2. FIGURE : ESTIMATED POWER
3. FIGURE : PERCENTAL ERROR

0.349 0.348 -0.3								
0.431 0.416 -3.5	0.485 0.461 -4.9							
0.631 0.621 -1.6	0.636 0.631 -0.8	0.572 0.569 -0.5						
0.797 0.793 -0.5	0.893 0.904 1.2	0.604 0.583 -3.5	0.708 0.687 -3.0					
0.931 0.929 -0.2	0.964 0.961 -0.3	1.067 1.082 1.4	0.903 0.905 0.2	0.778 0.777 -0.1				
1.019 1.018 0.0	1.218 1.236 1.5	1.111 1.108 -0.3	1.188 1.206 1.5	0.776 0.757 -2.4	0.923 0.901 -2.4			
1.011 1.004 -0.7	1.103 1.098 -0.5	1.327 1.337 0.8	1.183 1.176 -0.6	1.281 1.301 1.6	1.176 1.174 -0.2	1.440 1.447 0.5		
0.892 0.889 -0.3	1.142 1.154 1.1	1.156 1.145 -1.0	1.343 1.353 0.7	1.158 1.162 0.3	1.346 1.370 1.8	1.301 1.295 -0.5	1.481 1.495 0.9	
0.562 0.554 -1.4	0.705 0.674 -4.4	1.215 1.234 1.6	1.117 1.118 0.1	0.934 0.932 -0.2	0.865 0.849 -1.8	1.396 1.429 2.4	1.244 1.250 0.5	1.016 1.018 0.2

Fig. 3.4.3. Power distribution of test problem. No detectors.

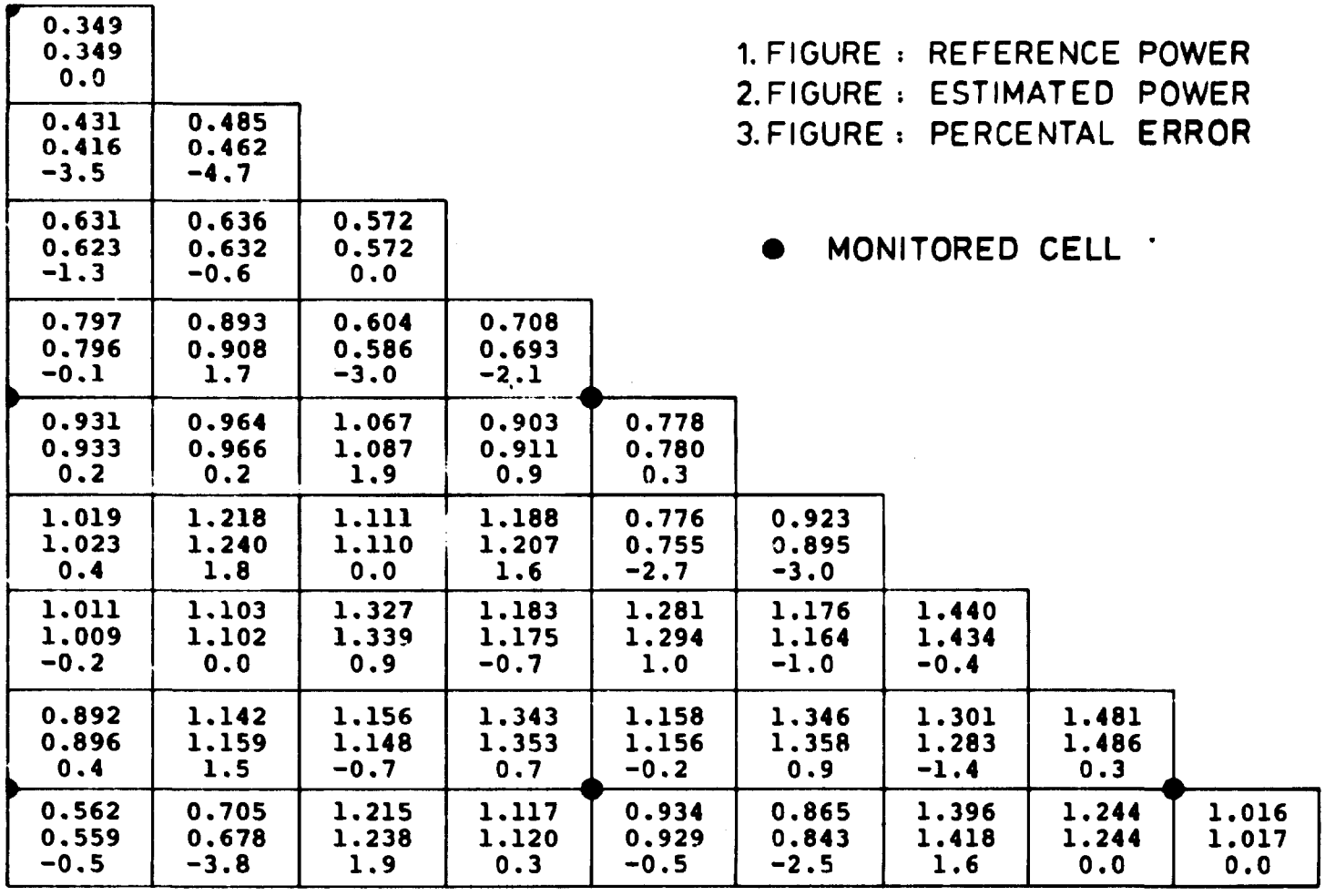

0.349 0.349 0.0								
0.431 0.416 -3.5	0.485 0.462 -4.7							
0.631 0.623 -1.3	0.636 0.632 -0.6	0.572 0.572 0.0						
0.797 0.796 -0.1	0.893 0.908 1.7	0.604 0.586 -3.0	0.708 0.693 -2.1					
0.931 0.933 0.2	0.964 0.966 0.2	1.067 1.087 1.9	0.903 0.911 0.9	0.778 0.780 0.3				
1.019 1.023 0.4	1.218 1.240 1.8	1.111 1.110 0.0	1.188 1.207 1.6	0.776 0.755 -2.7	0.923 0.895 -3.0			
1.011 1.009 -0.2	1.103 1.102 0.0	1.327 1.339 0.9	1.183 1.175 -0.7	1.281 1.294 1.0	1.176 1.164 -1.0	1.440 1.434 -0.4		
0.892 0.896 0.4	1.142 1.159 1.5	1.156 1.148 -0.7	1.343 1.353 0.7	1.158 1.156 -0.2	1.346 1.358 0.9	1.301 1.283 -1.4	1.481 1.486 0.3	
0.562 0.559 -0.5	0.705 0.678 -3.8	1.215 1.238 1.9	1.117 1.120 0.3	0.934 0.929 -0.5	0.865 0.843 -2.5	1.396 1.418 1.6	1.244 1.244 0.0	1.016 1.017 0.0

Fig. 3.4.4. Power distribution of test problem. A quarter of the cells monitored.

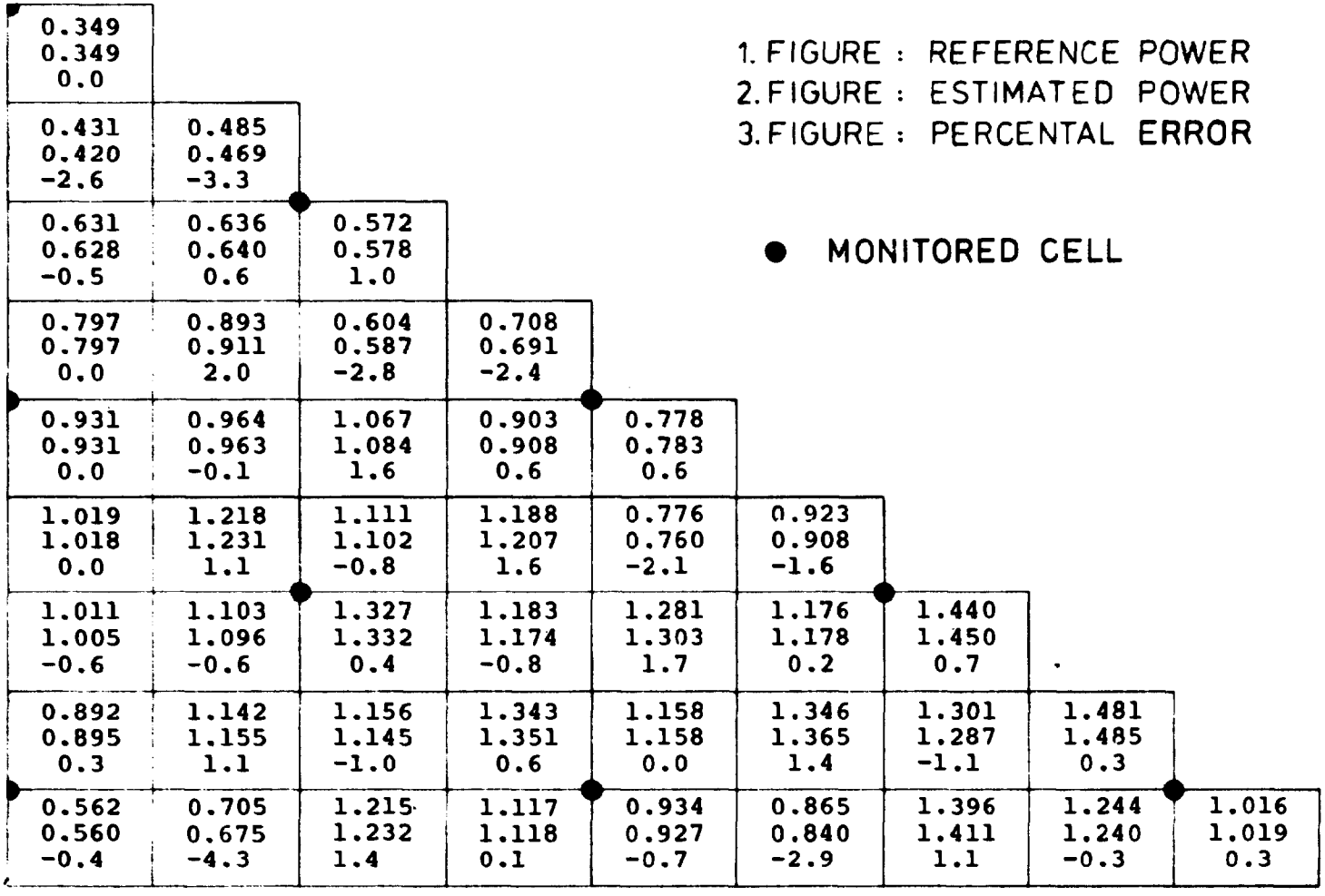

0.349 0.349 0.0								
0.431 0.420 -2.6	0.485 0.469 -3.3							
0.631 0.628 -0.5	0.636 0.640 0.6	0.572 0.578 1.0						
0.797 0.797 0.0	0.893 0.911 2.0	0.604 0.587 -2.8	0.708 0.691 -2.4					
0.931 0.931 0.0	0.964 0.963 -0.1	1.067 1.084 1.6	0.903 0.908 0.6	0.778 0.783 0.6				
1.019 1.018 0.0	1.218 1.231 1.1	1.111 1.102 -0.8	1.188 1.207 1.6	0.776 0.760 -2.1	0.923 0.908 -1.6			
1.011 1.005 -0.6	1.103 1.096 -0.6	1.327 1.332 0.4	1.183 1.174 -0.8	1.281 1.303 1.7	1.176 1.178 0.2	1.440 1.450 0.7		
0.892 0.895 0.3	1.142 1.155 1.1	1.156 1.145 -1.0	1.343 1.351 0.6	1.158 1.158 0.0	1.346 1.365 1.4	1.301 1.287 -1.1	1.481 1.485 0.3	
0.562 0.560 -0.4	0.705 0.675 -4.3	1.215 1.232 1.4	1.117 1.118 0.1	0.934 0.927 -0.7	0.865 0.840 -2.9	1.396 1.411 1.1	1.244 1.240 -0.3	1.016 1.019 0.3

Fig. 3.4.5. Power distribution of test problem. Half of the cells monitored.

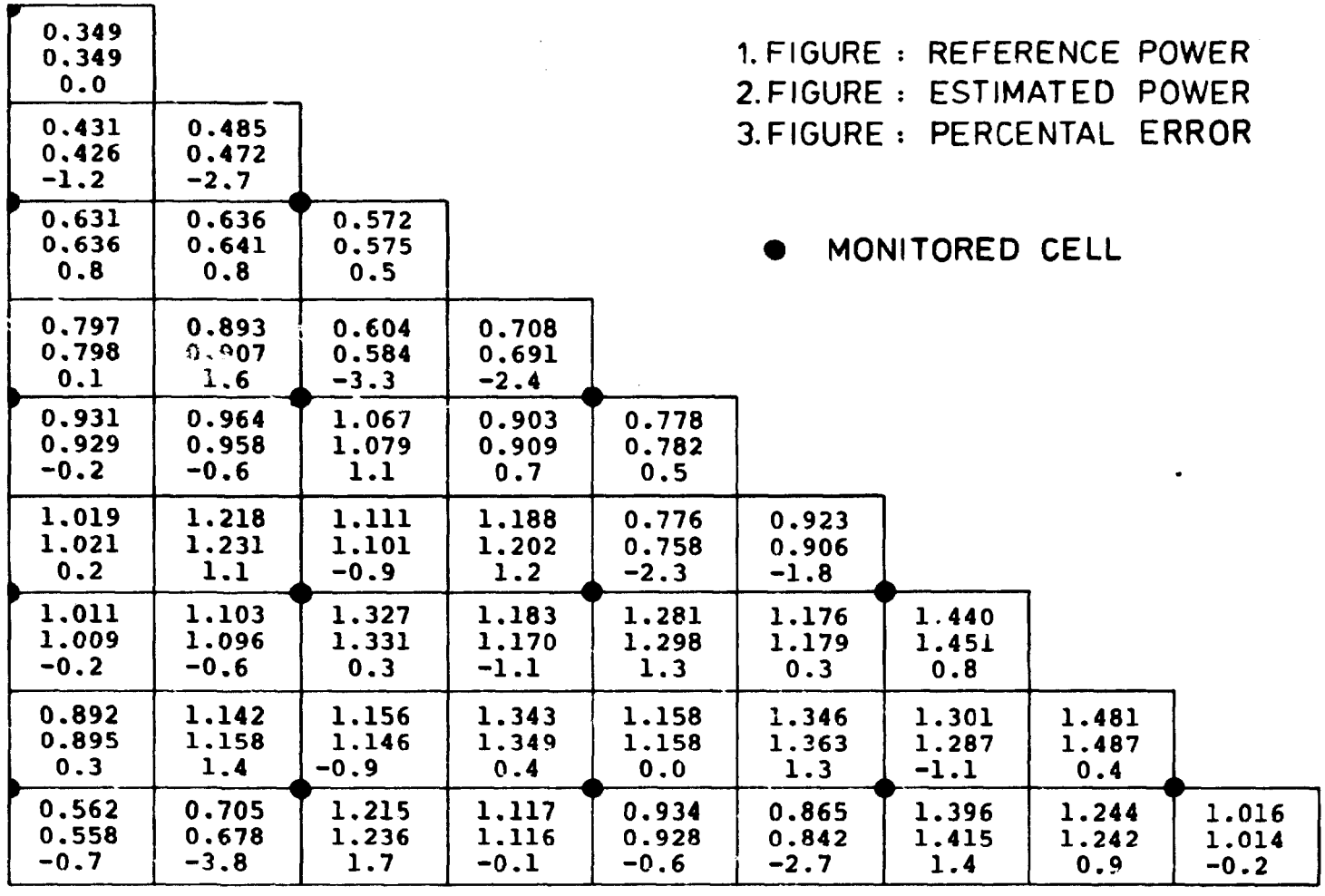

Fig. 3.4.6. Power distribution of test problem. All cells monitored.

4. ACCELERATED NODAL THEORY

4.1. The three-dimensional calculational method

The methods described in Sections 2 and 3 both require axially movable in-core detectors to get the three-dimensional power distribution. In contrast, the method presented in this section requires only fixed in-core detectors. Nodal theory has been chosen for the procedure partly because of the limited storage requirement and partly because of the modest computing time.

Taking the boxes of the reactor in cells of four boxes, approximately one-quarter of the cells are equipped with detectors. The procedure starts by calculating the readings that would have been measured in the cells lacking instrumentation, if they were instrumented. These pseudo readings are calculated at each detector level. The calculation is performed for the horizontal plane at that level in two dimensions and comprises outer iterations, where the eigenvalue is adjusted, and inner iterations, where the flux values are determined. Axial leakage is neglected. In the inner iterations, the fluxes of the instrumented cells are replaced by auxiliary variables, and the equations are solved for these. The cell powers are calculated, and the auxiliary variables are normalized, so that calculated and measured values agree. Having determined readings, pseudo or real, for all cells in the reactor, the axial power distribution of each cell is calculated using these readings. The power distribution for a cell is calculated using the detector readings of that cell alone. Each cell consisting of four boxes with zero, one, or two control rods inserted is homogenized. A one-channel calculation is performed in which the detector readings are used to modify the boundary conditions in the horizontal direction. Initially, reflecting boundary conditions are used. The power distribution corresponding to reflecting boundary conditions will produce detector readings different from the real ones. The deviation between real and calculated readings is a measure of the leakage

in the horizontal direction. Therefore, the boundary conditions are altered iteratively according to this deviation so as to produce a power distribution giving the same values for the measured and calculated readings. The fuel box power is calculated using the axial power distribution of the cell to which it belongs. The box power is calculated by multiplying the cell power by predetermined correlation factors.

The method described above has been applied to a quarter core of a boiling water reactor. The whole core consists of 444 fuel bundles. The total coolant flow rate of the core is 5750 kg/s, and the thermal power of the reactor is 1707 MW. The control rod pattern is shown in Fig. 4.1.1. and the numbering of hydraulic channels in Fig. 4.1.2. The detector arrangement in the horizontal plane is shown in Fig. 4.1.3. Eight cells are monitored and 16 are unmonitored. Most of the peripheral boxes do not belong

22							20	20		
	61	61			87	87				
	61	61			87	87				
			14	14			7	7		
			14	14			7	7		
	96	96			54	54				
	96	96			54	54				
20			7	7						
20			7	7						

Fig. 4.1.1. Control rod pattern. The numbers indicate the insertion in per cent.

1	2	3	4	5	6	7	8	9	10	11
12	13	14	15	16	17	18	19	20	21	22
23	24	25	26	27	28	29	30	31	32	33
34	35	36	37	38	39	40	41	42	43	44
45	46	47	48	49	50	51	52	53	54	55
56	57	58	59	60	61	62	63	64	65	66
67	68	69	70	71	72	73	74	75	76	77
78	79	80	81	82	83	84	85	86	87	
88	89	90	91	92	93	94	95	96		
97	98	99	100	101	102	103	104			
105	106	107	108	109	110	111				

Fig. 4.1.2. Numbering of hydraulic channels.

to any cell. The detector arrangement in the vertical direction is shown in Fig. 4.1.4. The detectors are located at 4 axial levels. Each box is divided into 25 nodes. A detector is located 4, 10, 16, and 22 nodes from the bottom. The axial levels are named A, B, C, and D, respectively. The detector readings used as input to the calculational procedure are the average power of the four nodes surroundings the detectors and are provided by a three-dimensional nodal theory calculation, also serving as the reference case.

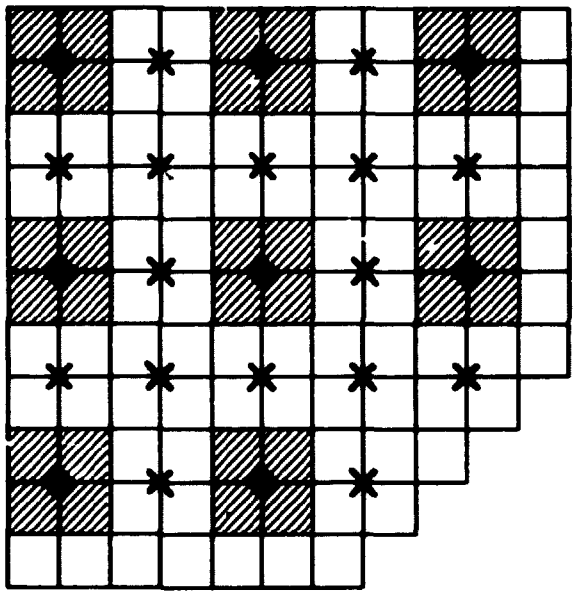

● MONITORED CELL
✕ UNMONITORED CELL

Fig. 4.1.3. Detector arrangement in the horizontal plane.

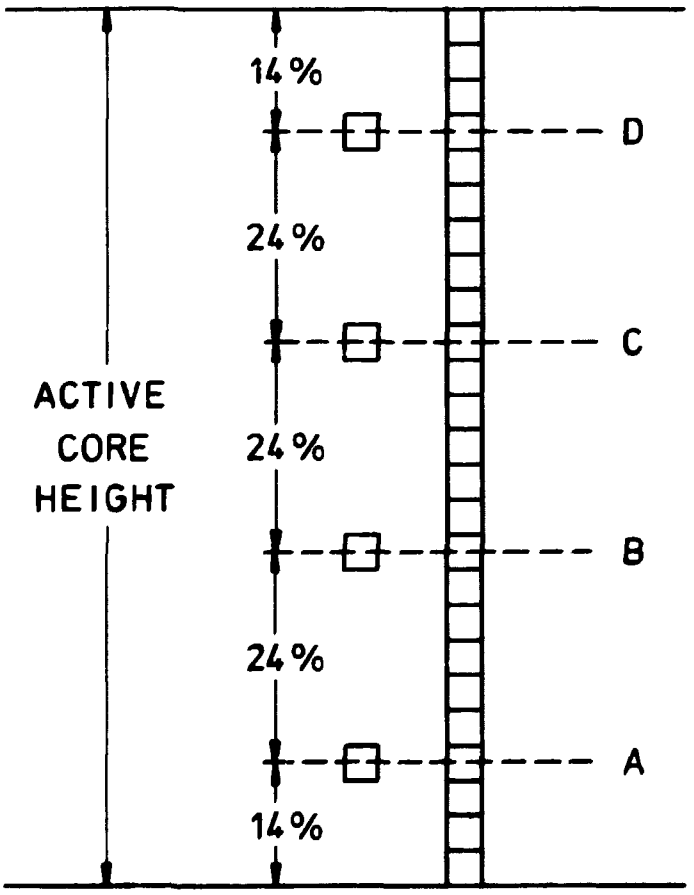

Fig. 4.1.4. Detector arrangement in the vertical direction.

4.2. An alternative approach

Nodal theory calculations coupled with detector readings have been based on the FLARE model [7,8,9,10]. In this method three-dimensional calculations are performed in each cell, and the coupling between the cells is expressed in terms of an albedo derived from two-dimensional calculations. Two-dimensional calculations are also used to calculate pseudo-detector readings of unmonitored cells. In this way monitored and unmonitored cells can be treated similarly.

For monitored cells the basic equation of the nodal coupling method is

$$S_i(\kappa) = \frac{k_{\infty i}(\kappa)}{\lambda} \left(W^v{}_i(\kappa + 1)S_i(\kappa +1)+ W^v{}_i(\kappa - 1)\ S_i(\kappa -1)\right.$$

$$+ \sum_{j \neq i}^{2} W^h{}_j(\kappa)S_j(\kappa)$$

$$\left. + \{1 - 2W^v{}_i(\kappa)-(4 - \alpha_i(\kappa))W_i{}^H(\kappa)\ \}\ S_i(\kappa)\right) \qquad (4.2.1)$$

where

i = index of a fuel bundle in a real-monitored cell

j = index of a fuel bundle adjacent to i in a real-monitored cell

κ = axial node number

$S_i(\kappa)$ = neutron source

$\kappa_{\infty i}(\kappa)$ = infinite neutron multiplication factor eigenvalue

$W^v{}_i(\kappa)$ = vertical neutron transport kernel

$W_i{}^h(\kappa)$ = horizontal neutron transport kernel

$\alpha_i(\kappa)$ = horizontal albedo (2.0) for flat boundary condition

This equation can be solved only when the albedo $\alpha_i(\kappa)$ is known. A first estimate of the albedo can be made by performing a two-dimensional calculation that provides the relative magnitudes of the $S_i(\kappa)$ of neighbouring fuel bundles. The calculation is done at each axial level of nodes.

The power distribution of the monitored cell is determined from the first estimate of the albedo. The detector readings corresponding to this power distribution are calculated and compared with the true detector readings. In case of a discrepancy the albedo is adjusted using the equation

$$\alpha_i(\kappa_n)(\text{new}) = (1 + \epsilon\ \delta(\kappa_n))\ \alpha_i(\kappa)\ (\text{old})$$

$$n = 1, 2, 3, 4, \qquad (4.2.2)$$

where $\delta(\kappa_n)$ s the correction factor at an axial node κ_n at which the nth detector is located, and ϵ is the overestimate relaxation factor. The factor $\delta(\kappa_n)$ is calculated by

$$\delta(\kappa_n) = \frac{\phi_m(k_n) - \phi_c(k_n)}{0.25\ \phi_m(k_n)} \qquad (4.2.3)$$

where $\phi_m(\kappa_n)$ and $\phi_c(\kappa_n)$ are the measured and calculated detector readings, respectively. The correction factors at the other axial nodes, where detectors are not located, are determined by linear interpolation or extrapolation of $\delta(\kappa_n)$ with some correction made at the control rod tips. The correction of $\alpha_i(\kappa_n)$ is repeated until the differences between the calculated and measured detector readings become small enough.

When all monitored cells have been treated in this way, the detector readings that would have been measured in the unmonitored cells, if they were instrumented, are calculated. At each axial detector level a two-dimensional equation is solved using the neutron source of monitored cells as the fixed source

$$S_i^{(n)}(\kappa_n) = \frac{\kappa_{\infty i}(\kappa_n)}{\lambda} \Big[\sum_{j \neq i} W_j^h(\kappa_n)\, S_j^{(n)}(\kappa_n)$$

$$+ \sum_{j \neq i} W_j^h(\kappa_n)\, S_j^{(m)}(\kappa_n)$$

$$+ \{1 - 4\, W_i^h(\kappa_n) - (2 - \beta_i(\kappa_n))\}\, S_i^{(n)}(\kappa_n) \Big] \qquad (4.2.4)$$

where $\beta_i(\kappa_n)$ is the vertical albedo; the superscript m indicates the monitored cells and n the unmonitored cells. The vertical albedo is estimated using the equation

$$\beta_i(\kappa_n) = \frac{W_i^V(\kappa_n+1) S_i^{(n)}(\kappa_n+1) + W_i^V(\kappa_n-1) S_i^{(n)}(\kappa_n-1)}{W_i^V(\kappa_n) S_i^{(n)}(\kappa_n)} \qquad (4.2.5)$$

Since $S_i^{(n)}(\kappa_n)$, $S_i^{(n)}(\kappa_n + 1)$ and $S_i^{(n)}(\kappa_n - 1)$ are unknown until the equation has been solved, the values of the bundle of the monitored cell nearest to bundle i are used instead.

Now, the scheme for monitored cells can be applied to the unmonitored ones as well, and in this way the global power distribution can be determined.

4.3. The TRILUX model

The TRILUX model [11] is based upon nodal theory, like the FLARE model presented in Section 4.2. It is, however, more advanced, the difference being an increased number of coupling coefficients. The coupling coefficients are

r_{ij} = the fraction of neutrons leaving node i and entering node j

σ_j = the probability that a neutron born in node j is absorbed in node j

ρ_j = the probability that node j directly reflects a neutron streaming into node j

β_j = the probability that node j absorbs a neutron streaming into node j

μ_j = the probability that a neutron entering node j behaves like neutrons already present in node j

A neutron from node i is either reflected by node j or absorbed in node j or enters node j without being absorbed. In case a neutron enters node j without being absorbed it behaves like neutrons born in node j. Consequently, the following relation applies:

$$\mu_j + \rho_j + \beta_j = 1 \qquad (4.3.1)$$

The following variables are introduced:

M_j = the fictive source comprising the fission source and the neutrons streaming into node j

S_j = the fission source

J_j^{in} = the neutron current into the j-th node

S_j and M_j are related by

$$M_j = S_j + \mu_j J_j^{in} \qquad (4.3.2)$$

In a steady state one has furthermore

$$S_j = (\sigma_j M_j + \beta_j J_j^{in})k_j \qquad (4.3.3)$$

k_j being the infinite multiplication factor for node j. Now, J_j^{in} is eliminated from these two equations, the result being

$$J_j^{in} = \frac{1-\sigma_j k_j}{k_j(\beta_j+\sigma_j\mu_j)} S_j \qquad (4.3.4)$$

$$S_j = \frac{k_j(\alpha_j+\sigma_j)}{1+\alpha_j k_j} M_j \qquad (4.3.5)$$

where

$$\alpha_j = \beta_j/\mu_j \tag{4.3.6}$$

The eigenvalue λ is introduced replacing k_j by k_j/λ

$$S_j = \frac{k_j(\alpha_j+\sigma_j)}{\lambda+\alpha_j k_j} M_j \tag{4.3.7}$$

The leakage from node i to node j is $W_{ji}\ M_i$.

The coupling coefficients W_{ji} can be expressed in terms of the other coefficients. An "i"-neutron becomes a "j"-neutron when the following conditions are satisfied:

1. The neutron must not be absorbed in node i; the probability of this is $1 - \sigma_i$.

2. The neutron must arrive at node j, when leaving i; the probability of this is r_{ij}.

3. The neutron must not be reflected by node j; the probability of this is $1 - \rho_j$.

If the neutron is directly reflected, there is still a possibility for it to become a "j"-neutron, in case it is reflected by node i again. Thus W_{ji} is seen to be equal to

$$\begin{aligned} W_{ji} &= r_{ij}(1 - \sigma_i) \\ &\quad \cdot((1 - \rho_j)+ \rho_j\ \rho_i(1 - \rho_j)+ \rho_j^2\ \rho_i^2(1 - \rho_j)+\ldots) \\ &= r_{ij}(1 - \sigma_i)(1 - \rho_j) \sum_{n=0}^{\infty} \rho_j^n\ \rho_i^n = \\ &= r_{ij}(1 - \sigma_i)(1 - \rho_j)/(1 - \rho_j\ \rho_i) \end{aligned} \tag{4.3.8}$$

The leakage from i to node j is

$$W_{ji} M_i = \frac{1+\alpha_i k_i}{k_i(\alpha_i+\sigma_i)} r_{ij} \frac{(1-\sigma_i)(1-\rho_j)}{1-\rho_j\rho_i} S_i \qquad (4.3.9)$$

The neutron balance equation states that leakage and absorption must equal production. The production term for node j is simply S_j, and the absorption term is S_j/k_j. Thus the neutron balance equation becomes

$$\Sigma W_{ij} M_j - \Sigma W_{ji} M_i + S_j/k_j = S_j \qquad (4.3.10)$$

The summation is extended over the six neighbour nodes of node j. Using the relation between S_j and M_j the equation may be expressed in terms of M_i and M_j alone

$$\Sigma W_{ij} M_j - \Sigma W_{ji} M_i + \frac{k_j(\sigma_j+\alpha_j)}{1+\alpha_j k_j} (1/k_j-1)M_j \qquad (4.3.11)$$

Again, the eigenvalue λ is introduced replacing k_j by k_j/λ, and thus

$$\Sigma W_{ij} M_j - \Sigma W_{ji} M_i + \frac{k_j(\sigma_j+\alpha_j)}{\lambda+\alpha_j k_j} (\lambda/k_j-1)M_j = 0 \qquad (4.3.12)$$

W_{ji} may be written

$$W_{ji} = (1 - \sigma_i)W_{ji}' \qquad (4.3.13)$$

where

$$W_{ji}' = \frac{1+\alpha_i k_i}{k_i(\alpha_i+\sigma_i)} r_{ij} \frac{1-\rho_j}{1-\rho_j\rho_i} \qquad (4.3.14)$$

When j and i are both in-core nodes ρ_j and ρ_i will not differ much, and the following approximation is used

$$\frac{1-\rho_j}{1-\rho_j\rho_i} \equiv \frac{1-\rho_j}{1-\rho_j^2} = \frac{1}{1+\rho_j} \qquad (4.3.15)$$

In the event that j is an in-core node and i a reflector node ρ_i will be very different from ρ_j, and the above approximation is not made. The value to be used for ρ_i will be the albedo.

In terms of W_{ji}' and W_{ij}' the neutron balance equation becomes

$$\Sigma W_{ij}'(1 - \sigma_j)M_j - \Sigma W_{ji}'(1 - \sigma_i)M_i + \frac{k_j(\sigma_j+\alpha_j)}{\lambda+ \alpha_j k_j} (\lambda/k_j - 1)M_j = 0 \qquad (4.3.16)$$

A new variable U_j is introduced by

$$U_j = (1 - \sigma_j)M_j \qquad (4.3.17)$$

and in terms of this variable the neutron balance equation is

$$\Sigma W_{ij}' U_j - \Sigma W_{ji}' U_j + \frac{k_j(\sigma_j+\alpha_j)}{\lambda+\alpha_j k_j} \frac{(\lambda/k_j-1)}{1-\sigma_j} U_j = 0 \qquad (4.3.18)$$

4.4.1. Method for calculating estimated detector readings of cells without instrumentation

Consider a cell of nodes surrounded by four cells. Then the nodes of that cell are referred to as internal, whereas nodes of other cells are named external with respect to that cell. The readings that would have been measured in the cells without detectors if they were instrumented are estimated by solving the two-dimensional TRILUX equation:

$$\Sigma W_{ij}' U_j - \Sigma W_{ji}' U_i + \frac{k_j(\sigma_j+\alpha_j)}{\lambda+\alpha_j k_j} \frac{(\lambda/k_j-1)}{1-\sigma_j} U_j = 0 \qquad (4.4.1)$$

at an axial detector level. In using the two-dimensional equation instead of the three-dimensional one, axial leakage is neglected. The equation is to be solved with the additional constraint that the calculated detector readings of the instrumented cells coincide with the true detector readings.

Now, let node j be an internal node. The leakage from the neighbour nodes $\Sigma W_{ji} U_i$ is split up in the following way

$$\Sigma W_{ji}' U_i = \sum_{ext} W_{ji}' U_i + \sum_{int} W_{ji}' U_i \qquad (4.4.2)$$

where the first summation on the right-hand side extends over external nodes and the second over internal nodes. This expression is inserted in the TRILUX equation, and the term $\sum_{ext} W_{ji}' U_i$ is moved to the right-hand side of that equation yielding

$$\sum W_{ij}' U_j - \sum_{int} W_{ji}' U_j + \frac{k_j(\sigma_j+\sigma_j)}{\lambda+\alpha_j k_j} \frac{(\lambda/k_j-1)}{1-\sigma_j}$$

$$= \sum_{ext} W_{ji}' U_i \qquad (4.4.3)$$

The left-hand side of this equation contains contributions from internal fission sources only and the right-hand side from external sources only. The equation must be solved so that the detector reading calculated on the basis of the fission source is equal to the measured reading, if the cell is instrumented,

$$\int_{int} E_o S_j/\nu_j \cdot \Omega_j = P \qquad (4.4.4)$$

where

E_o = the energy released per fission

ν_j = number of neutrons produced per fission

Ω_j = volume of node j

P = detector reading

Expressed in terms of U_j, the additional condition becomes

$$\int_{int} E_o \frac{k_j(\alpha_j+\sigma_j)}{\lambda+\alpha_j k_j} \frac{1}{1-\sigma_j} \frac{U_j}{\nu_j} \Omega_j = P \qquad (4.4.5)$$

If an attempt is made at solving the equation system as it is formulated above, no solution will be found since it is overdetermined. This difficulty may be resolved by substituting the auxiliary variables V_i and V_j for U_i and U_j on the left-hand side of the TRILUX equation. The result is

$$\sum W_{ij}' V_j - \sum_{int} W_{ji}' V_i + \frac{k_j(\sigma_j+\alpha_j)}{\lambda+\alpha_j k_j} \frac{(\lambda/k_j-1)}{1-\sigma_j} V_j$$

$$= \sum_{ext} W_{ji}' U_i \qquad (4.4.6)$$

Setting this equation up for all boxes in the reactor one gets a set of coupled equations of the form

$$A_{int} \; V_{int} = \sum_{n} A_{ext}^{n} \; U_{ext}^{n} \qquad (4.4.7)$$

where

A_{int} = 4 x 4 matrix of coefficients for internal boxes

V_{int} = vector of four internal auxiliary variables

n = index denoting one of four cells neighbouring the cell under consideration

A_{ext}^{n} = 4 x 4 matrix of coefficients for external boxes of cell n neighbouring the cell under consideration

U_{ext}^{n} = vector of four external variables of cell n neighbouring the cell under consideration

U_{int} = vector of four internal variables

There are as many equation systems of this form as there are cells in the reactor. When an internal vector U_{int} has been found this will be an external vector U_{ext}^{n} to the neighbouring cells.

The equations are solved as follows: The eigenvalue λ and the vectors U_{int} and U_{ext}^{n} are set equal to

λ = 1

U_{int} = (1, 1, 1, 1)

$$U_{ext}^{n} = (1, 1, 1, 1) \quad n = 1, 2, 3, 4$$

$$V_{int} = (1, 1, 1, 1)$$

for all cells in the reactor. Then the solution proceeds as follows

1. For instrumented cells:
   The vector V_{int} is found using

$$V_{int} = \sum A_{int}^{-1} A_{ext}^{n} U_{ext}^{n} \qquad (4.4.8)$$

   Then the normalization factor N is determined so that

$$N \sum_{int} E_o \frac{k_j(\alpha_j+\sigma_j)}{\lambda+\alpha_j k_j} \frac{1}{\nu_j} \frac{1}{1-\sigma_j} \Omega_j V_j = P \qquad (4.4.9)$$

Finally, the vector U_{int} is found using

$$U_{int} = N V_{int} \qquad (4.4.10)$$

2. For cells without instrumentation:
   No normalization is required, and the equation system is

$$A_{int} U_{int} = \sum_{n} A_{ext}^{n} U_{ext}^{n} \qquad (4.4.11)$$

   with the solution

$$U_{int} = \sum A_{int}^{-1} A_{ext}^{n} U_{ext}^{n} \qquad (4.4.12)$$

When U_{int} has been found for a cell, instrumented or not, the corresponding vectors U_{ext}^{n} of neighbouring cells are set equal to U_{int}.

When all cells have been treated, the average value of the normalizing factors of the instrumented cells is found, and the vectors U_{int} of the cells without instrumentation is multiplied by this value. A new estimate of the eigenvalue is made, and the

procedure is repeated, until both the eigenvalue and vectors U_{int} converge.

The eigenvalue is estimated as follows: Consider the equation for node j

$$V_j(\sum W_{ij}' + \frac{\alpha_j+\sigma_j}{\lambda+\alpha_j k_j}\frac{\lambda-k_j}{1-\sigma_j}) - \sum_{int} W_{ji}' V_i = \sum_{ext} W_{ji}' U_i \qquad (4.4.13)$$

U_j and V_j are related by $V_j = 1/N\ U_j$ which, on insertion into the equation above, gives

$$1/N\ U_j \sum W_{ij}' + 1/N/k_j\ S_j(\lambda-k_j) - 1/N \sum_{int} W_{ji}' U_i = \sum_{ext} W_{ji}' U_i \qquad (4.4.14)$$

From both the right- and left-hand side of this equation, $N \Sigma\ W_{ji}' U_i$ is subtracted yielding

$$U_j \sum W_{ij}' + \lambda\ S_j/k_j - S_j \sum W_{ji}' U_i = (N-1) \sum_{ext} W_{ji}' U_i \qquad (4.4.15)$$

N is replaced by N_j since it differs for nodes of different cells. The equations are summed up for the whole core, and the result reduces to

$$\sum_i (S_j - U_j \sum_R W_{ij}' - \lambda\ S_j/k_j) = \sum_j (N_j-1) \sum_{ext} W_{ji}' U_i \qquad (4.4.16)$$

where $\sum_R$ denotes summation over all nodes adjacent to the reflector. From this λ is estimated to

$$\lambda = \frac{\sum_j \{S_j - U_j \sum_R W_{ij}' - (N_j-1) \sum_{ext} W_{ji}' U_i\}}{\sum_j S_j/k_j} \qquad (4.4.17)$$

4.4.2. Results of calculating estimated detector readings of cells without instrumentation

The coupling coefficients of the TRILUX equation are dependent on the fuel temperature and the void fraction both of which are unknown. For the fuel temperature the average value over the core which is 597°C has been used. For the void fraction a value of 10% has been chosen for axial level A, 40% for axial level B, 60% for axial level C, and 70% for axial level D. The choice of these values is not critical, but assuming the same value for all nodes at a given detector level will make the estimated readings different from those determined by a three-dimensional nodal theory calculation, since the void fraction varies from node to node. In general, the void fraction of boxes with a control rod inserted will be lower than the average value at a given detector level. The estimated reading of a cell is equal to the average power of the boxes of the cell.

The estimated detector readings of axial level A are shown in Fig. 4.4.1. Detector level A is situated at node 4 from the bottom. The control rod pattern is characterized by 7 cells with two control rods, 11 cells with one control rod, and 6 cells without control rods. The standard deviation of the per cent error is 4.4%. The greatest errors occur for the cell consisting of channels 7, 8, 18, and 19, where it is -9.1%, and the cell consisting of channels 31, 32, 42, and 43, where it is also -9.1% and the symmetrically located cells. The cell consisting of channels 7, 8, 18, and 19 has two control rods inserted at node 5 and 22 from the bottom. Thus the tip of one of the control rods is only one node from level A, meaning that neutrons will leak in from above. This three-dimensional effect cannot be taken into account in the two-dimensional calculation. Moreover, the presence of two control rods will make the void fraction less than the average void fraction at detector level A. Neglecting axial leakage and assuming a void fraction which is too big will both reduce the estimated detector readings as compared with the three-dimensional nodal theory calculation. The cell consisting of channels 31, 32, 42, and 43 has one control rod inserted 2 nodes. Thus the tip of the control rod is only 1 node

+ 0.790 1.072	1.068 1.052	+ 1.110 1.030	0.961 0.873	+ 1.203 1.009
1.069 1.061	1.041 1.022	1.081 1.074	1.263 1.280	1.503 _.623
+ 1.111 1.029	1.082 1.075	+ 1.119 0.995	1.292 1.313	+ 1.484 0.926
0.962 0.874	1.265 1.285	1.293 1.315	1.234 1.253	1.180 1.197
+ 1.207 1.012	1.514 1.625	+ 1.486 0.928	1.180 1.197	

1. FIGURE: EXACT DETECTOR READING
2. FIGURE: ESTIMATED DETECTOR READING FOR UNMONITORED CELLS
   NORMALIZING FACTOR FOR MONITORED CELLS

\+ MONITORED CELL

Fig. 4.4.1. Estimated detector readings of detector level A.

from level A, meaning that neutrons will leak out. In addition, the boxes 32 and 43 have a coolant rate much less than the average box coolant rate due to the throttling, so that the void fraction is greater than the average void fraction. Therefore, the estimated detector reading of this cell is overpredicted. Four of the cells with two control rods have a control rod inserted 3.5 nodes. Although the control rod tips are situated at detector level A, the estimated detector readings are nevertheless in fairly good agreement with the three-dimensional nodal theory calculation. Neglecting axial leakage will raise the estimated reading whereas use of the average void fraction will reduce it, because the void fraction is lower than the average value, and so these effects tend to offset each other.

The estimated detector readings of axial level B are shown in Fig. 4.4.2. Axial level B is situated 10 nodes from the bottom. The control rod pattern is characterized by 16 cells with one control rod and 8 cells without control rods. The standard deviation of the per cent error is 5.6%. The greatest errors occur in the cell consisting of channels 31, 32, 42, and 43, where it is 8.1%, in the cell consisting of channels 73, 74, 84, and 85, where it is -10%, in the cell consisting of channels 75, 76, 86, and 87, where it is -9.4%, and in the symmetrically located cells. The control rod tip just below axial level B is situated at node 6, and the control rod tip just above B is found at node 14. Thus no three-dimensional effect due to control rods is likely at axial level B. It appears from Fig. 4.4.2 that most of the estimated detector readings are underpredicted. This is due to the control rods which reduce the void fraction.

The estimated detector readings of axial level C are shown in Fig. 4.4.3. Axial level C is situated 16 nodes from the bottom. The control rod pattern is characterized by 12 cells with one control rod and 12 cells without a control rod. The standard deviation of the percental error is 5.3%. The greatest error occurs in the cell consisting of channels 75, 76, 86, and 87, where it is -8.9%. Four of the cells have a control rod tip situated at detector level C, and the impact on the estimated detector readings is evident.

+ 1.176 1.023	1.111 1.112	+ 1.116 1.013	1.209 1.140	+ 1.276 0.966
1.111 1.112	1.125 1.089	1.127 1.097	1.132 1.112	1.170 1.265
+ 1.117 1.011	1.127 1.097	+ 1.111 1.043	1.068 1.027	+ 1.078 0.979
1.210 1.143	1.132 1.115	1.068 1.032	0.958 0.862	0.852 0.771
+ 1.276 0.967	1.182 1.260	+ 1.078 0.978	0.852 0.774	

1. FIGURE: EXACT DETECTOR READING
2. FIGURE: ESTIMATED DETECTOR READING FOR UNMONITORED CELLS
   NORMALIZING FACTOR FOR MONITORED CELLS

\+ MONITORED CELL

Fig. 4.4.2. Estimated detector readings of detector level B.

+ 1.959 0.962	1.739 1.848	+ 1.282 0.999	1.091 1.012	+ 1.031 1.018
1.734 1.838	1.636 1.723	1.317 1.319	1.134 1.091	1.018 1.034
+ 1.272 1.001	1.312 1.310	+ 1.522 1.007	1.397 1.363	+ 1.030 1.013
1.075 1.003	1.123 1.079	1.390 1.358	1.284 1.195	0.846 0.771
+ 1.014 1.017	1.013 1.020	+ 1.021 1.014	0.842 0.770	

1. FIGURE: EXACT DETECTOR READING
2. FIGURE: ESTIMATED DETECTOR READING FOR UNMONITORED CELLS
   NORMALIZING FACTOR FOR MONITORED CELLS

\+ MONITORED CELL

Fig. 4.4.3. Estimated detector readings of detector level C.

+ 1.522 0.974	1.383 1.435	+ 1.087 0.986	0.874 0.852	+ 0.677 0.992
1.327 1.363	1.249 1.283	1.041 1.048	0.857 0.849	0.656 0.674
+ 0.888 1.014	0.897 0.882	+ 0.990 1.003	0.881 0.868	+ 0.631 1.022
0.656 0.615	0.688 0.649	0.833 0.806	0.760 0.699	0.500 0.445
+ 0.572 1.024	0.580 0.573	+ 0.591 1.041	0.488 0.435	

1. FIGURE: EXACT DETECTOR READING
2. FIGURE: ESTIMATED DETECTOR READING FOR UNMONITORED CELLS
   NORMALIZING FACTOR FOR MONITORED CELLS

\+ MONITORED CELL

Fig. 4.4.4. Estimated detector readings of detector level D.

The estimated detector readings of axial level D are shown in Fig. 4.4.4. Axial level D is situated 22 nodes from the bottom. The control rod pattern is characterized by 8 cells with one control rod inserted and 16 without control rods. The standard deviation of the per cent error is 5.3%. The greatest error occurs in the cell consisting of channels 75, 76, 86 and 87, where it is -11.0%. Four of the cells have a control rod tip situated at detector level D. The deep insertion of the control rods in these cells causes the void fraction to become less than the average value at detector level D, and this counteracts the effect of axial leakage.

4.5.1. Method for calculating axial cell power distribution

When estimating the detector readings that would have been measured in cells without detectors if they were instrumented, a modified form of the TRILUX equation was solved neglecting axial leakage. This was justified by the homogeneous construction of boiling water reactors in the axial direction. When estimating axial cell power distributions on the basis of measured or calculated detector readings the one-dimensional TRILUX equation is used, but as a consequence of the greater variation in the radial direction radial leakage cannot be neglected, and the detector readings are taken care of in a different way. The cells consisting of four fuel boxes are homogenized. The one-dimensional equation is derived from the three-dimensional one in the following way: Consider the three-dimensional TRILUX equation for node j

$$U_j\left(\sum W_{ij}' + \frac{a_j+\sigma_j}{\lambda+a_jk_j}\,\frac{\lambda-k_j}{1-\sigma_j}\right) = \sum W_{ji}'\,U_i \qquad (4.5.1)$$

with the summation extending over the six neighbours of node j. Now, the sums on the right- and left-hand side of the equation are split into two parts, a vertical one and a horizontal one, comprising contributions from neighbour nodes belonging to the same cell and neighbour nodes belonging to the same axial level as node j.

$$\sum W_{ij}' = \sum_v W_{ij}' + \sum_h W_{ij}' \tag{4.5.2}$$

$$\sum W_{ji}' U_i = \sum_v W_{ji}' U_i + \sum_h W_{ji}' U_i \tag{4.5.3}$$

These expressions are inserted in the three-dimensional TRILUX equation, and the horizontal terms are moved to the left-hand side of the equation

$$U_j\left(\sum_v W_{ij}' + \sum_h W_{ij}' + \frac{\alpha_j+\sigma_j}{\lambda+\alpha_j k_j}\frac{\lambda-k_j}{1-\sigma_j}\right) - \sum_h W_{ji}' U_i$$

$$= \sum_v W_{ji}' U_i \tag{4.5.4}$$

The horizontal terms on the left-hand side are collected thus:

$$\sum_h W_{ij}' U_j - \sum_h W_{ji}' U_i = \sum_h W_{ij}' U_j\left(1 - \sum_h W_{ji}' U_i / \sum_h W_{ij}' U_j\right) \tag{4.5.5}$$

The reflection coefficient β is introduced by

$$\beta = \sum_h W_{ji}' U_i / \sum_h W_{ij}' U_j \tag{4.5.6}$$

In case of reflecting boundary conditions $W_{ji}' = W_{ij}'$ and $U_i = U_j$. This means that $\beta = 1$ and the term which expresses the influence of the surroundings vanishes. For $\beta \neq 1$ the one-dimensional TRILUX equation obtains

$$U_j\left(\sum_v W_{ij}' + \sum_h W_{ij}'(1-\beta) + \frac{\alpha_j+\sigma_j}{\lambda+\alpha_j k_j}\frac{\lambda-k_j}{1-\sigma_j}\right) = \sum_v W_{ji}' U_i \tag{4.5.7}$$

Putting

$$C = \frac{\alpha_j+\sigma_j}{\lambda+\alpha_j k_j}\frac{\lambda-k_j}{1-\sigma_j} \tag{4.5.8}$$

the equation is rewritten thus

$$U_j = \frac{\sum_v W_{ji}' U_i}{\sum_v W_{ij}' + \sum_h W_{ij}'(1-\beta) + C}$$

$$= \frac{\sum_v W_{ji}' U_i}{\sum_v W_{ij}' + C} \cdot \frac{1}{1 + \frac{\sum_h W_{ij}'}{\sum_v W_{ij}' + C}(1-\beta)} \qquad (4.5.9)$$

The term $\sum_v W_{ji}' U_i/(\sum_v W_{ij}' + C)$ is obtained from this formula when $\beta = 1$ is inserted. Therefore, U_{jo} is introduced putting

$$U_{jo} = \sum_v W_{ji}' U_i/(\sum_v W_{ij}' + C) \qquad (4.5.10)$$

Although radial leakage must be taken into account and β, therefore, is different from 1, in general, it will not deviate much from 1. Expanding the expression for U_j one gets to the first order in $1-\beta$:

$$U_j \approx U_{jo}\left(1 - \frac{\sum_h W_{ij}'}{\sum_v W_{ij}' + C}(1-\beta)\right) \qquad (4.5.11)$$

A change in β by $\Delta\beta$ will then be accompanied by a change in U_j given by

$$\Delta U_j \approx U_{jo} \frac{\sum_h W_{ij}'}{\sum_v W_{ij}' + C} \Delta\beta \qquad (4.1.12)$$

The correction factor $\sum_h W_{ij}'/(\sum_v W_{ij}' + C)$ varies around 2.0. The formula obtained suggests that the reflection coefficient should be adjusted in proportion to $\Delta U_j/U_j$. We thereby may in-

corporate the detector readings in the one-dimensional calculation in the following manner:

First β is set equal to 1 for all axial nodes, and the corresponding power distribution is determined. The deviation ΔP between calculated power P_c and measured power P_m is divided by P_m, and the reflection coefficient is adjusted according to the formula,

$$\Delta\beta = \frac{COR \cdot \Delta P/P_m}{XMAX} XLIM \qquad (4.5.13)$$

where XMAX denotes the maximum value at the detector locations of $COR \cdot \Delta P/P_m$ and XLIM is the maximum value of $\Delta\beta$. COR is a correction factor given by

$$COR = (\sum_v W_{ij}' + C)/\sum_h W_{ij}' \qquad (4.5.14)$$

At first XLIM is set equal to a predetermined value chosen in accordance with experience. This determines the values of $\Delta\beta$ at the detector locations. Where no detectors are situated, $\Delta\beta$ is found by linear interpolation or extrapolation of the values at the detector locations. The reflection coefficient is finally corrected using the formula,

$$\beta \text{ (new)} = \beta \text{ (old)} + \Delta\beta \qquad (4.5.15)$$

The power distribution corresponding to the new values of β is calculated, and the procedure described is repeated with a modified value of XLIM to be chosen in the following way: After each iteration the amount that $\Delta P/P_m$ has changed at the detector location with the greatest deviation in the previous iteration is examined. This change is denoted DXMAX. The sensitivity, SENS, is then found using SENS = XMAX/DXMAX. XLIM is changed depending on whether SENS is greater or less than 1

$$XLIM \text{ (new)} = 0.5 \; XLIM \text{ (old)} \quad \text{if SENS} < 1 \qquad (4.5.16)$$

$$XLIM \text{ (new)} = XLIM \text{ (old)} \quad \text{if SENS} > 1 \qquad (4.5.17)$$

In boiling water reactors the solution of the TRILUX equation is coupled with a thermal-hydraulic equation, which requires the thermal power and coolant flow rate of the cell. The thermal-hydraulic calculation provides the fuel temperature and the steam void distribution that strongly affects the power distribution. These values, however, are unknown until the three-dimensional power distribution has been calculated. With regard to the coolant flow rate, it is estimated by using the average flow rate per cell for the core. With regard to the thermal power, it is adjusted at the same time as the reflection coefficient by using the calculated and measured power at the detector locations

$$Q\ (\text{new}) = Q\ (\text{old})\ \frac{\Sigma\ P_m}{\Sigma\ P_c} \qquad (4.5.18)$$

where the summation is extended over all detector locations of the cell. As initial value the average thermal power per cell can be used. Since the coolant flow of a cell is the average of the four boxes in the cell, its variation is not as great as that of the box coolant flow, and differences due to throtting and the presence of control rods are reduced. Thus the assumption of average cell coolant flow seems justified.

The influence of the control rods is described using Henry's method[12] which implies that the fast and thermal absorption cross sections are corrected by a homogeneous poison cross section.

Since only the average axial power distribution of the cell is to be calculated, the four boxes of the cell are homogenized. At operating conditions a cell has one or two control rods inserted in it or non at all. In the event that one or two control rods are inserted it is necessary to know their weight in order to evaluate the absorption cross section of the cell. Therefore, a box calculation has been made with reflecting boundary conditions. The calculation presumes a box with no control rods inserted, one with a single control rod inserted, and four with one and two control rods inserted. The calculation was made at 0% void and a burnup of 0 MWd/tU. The following notation is introduced:

Σ_a(CELL) = absorption cross sectien for cell

Σ_a(CR) = absorption cross section for controlled box

Σ_a(NCR) = absorption cross section for uncontrolled box

X = weight factor for controlled box

The weight X is then determined from the following equation:

$$\Sigma_a(\text{CELL}) = X\ \Sigma_a(\text{CR}) + (1 - X)\ \Sigma_a(\text{NCR}) \qquad (4.5.19)$$

whence

$$X = \frac{\Sigma_a(\text{CELL}) - \Sigma_a(\text{NCR})}{\Sigma_a(\text{CR}) - \Sigma_a(\text{NCR})} \qquad (4.5.20)$$

The thermal absorption cross section Σ_{a2} and the fast absorption cross section Σ_{a1} for the various cases are given in the following table:

	$\Sigma_{a1}/\text{cm}^{-1}$	$\Sigma_{a2}/\text{cm}^{-1}$
1 box, 0 control rod	$2.21061 \cdot 10^{-2}$	$4.16696 \cdot 10^{-2}$
1 box, 1 control rod	$2.15240 \cdot 10^{-2}$	$6.30174 \cdot 10^{-2}$
4 boxes, 1 control rod	$2.20009 \cdot 10^{-2}$	$4.38073 \cdot 10^{-2}$
4 boxes, 2 control rods	$2.18726 \cdot 10^{-2}$	$4.63132 \cdot 10^{-2}$

From these results the following weight factors are derived:
For thermal absorption cross sections
no control rods per cell:

$$\Sigma_{a2}(\text{CELL}) = \Sigma_{a2}(\text{NCR}) \qquad (4.5.21)$$

one control rod per cell:

$$\Sigma_{a2}(\text{CELL}) = 0.09840 \cdot \Sigma_{a2}(\text{CR}) + 0.90160 \cdot \Sigma_{a2}(\text{NCR}) \qquad (4.5.22)$$

two control rods per cell:

$$\Sigma_{a2}(CELL) = 0.21754 \cdot \Sigma_{a2}(CR) + 0.78246 \cdot \Sigma_{a2}(NCR) \quad (4.5.23)$$

For fast absorption cross sections
no control rods per cell:

$$\Sigma_{a1}(CELL) = \Sigma_{a1}(NCR) \quad (4.5.24)$$

one control rod per cell:

$$\Sigma_{a1}(CELL) = 0.18072 \cdot \Sigma_{a1}(CR) + 0.81928\ \Sigma_{a1}(NCR) \quad (4.5.25)$$

two control rods per cell:

$$\Sigma_{a1}(CELL) = 0.40113 \cdot \Sigma_{a1}(CR) + 0.59887\ \Sigma_{a1}(NCR) \quad (4.5.26)$$

Calculations made at 75% void show that the change in these weight factors is negligible.

The eigenvalue λ is estimated in the following way: Let R denote the set of nodes belonging to the reflector and C the set belonging to the core. We first estimate λ for the general TRILUX equation and then for the modified one with the reflection coefficient β. Consider the following form of the TRILUX equation for node j

$$\sum_i W_{ji}' U_i - \sum_i W_{ij}' U_j + S_j - \lambda S_j/k_j = 0 \quad (4.5.27)$$

Summing over all nodes in the core, i.e. over C, one gets

$$\sum_{j\in C} \sum_i W_{ji}' U_i - \sum_{j\in C} \sum_i W_{ij}' U_j + \sum_{j\in C} S_j - \lambda \sum_{j\in C} S_j/k_j = 0 \quad (4.5.28)$$

where $j\in C$ means that node j is an element of class C. The two first terms on the left-hand side are split in the following manner:

$$\sum_{j\in C} \sum_i W_{ji}' U_i = \sum_{j\in C} \sum_{i\in C} W_{ji}' U_i + \sum_{j\in C} \sum_{i\in R} W_{ji}' U_i$$

$$= \sum_{j\in C} \sum_{i\in C} W_{ji}' U_i \quad (4.5.29)$$

Interchanging indices, the second term may be written:

$$\sum_{j\in C}\sum_{i} W_{ij}' U_j = \sum_{j\in C}\sum_{i\in C} W_{ij}' U_j + \sum_{j\in C}\sum_{i\in C} W_{ij}' U_j$$

$$= \sum_{j\in C}\sum_{i\in C} W_{ji}' U_i + \sum_{j\in C}\sum_{i\in R} W_{ij}' U_j \qquad (4.5.30)$$

Thus the difference between the two first terms reduces to

$$\sum_{j\in C}\sum_{i} W_{ji}' U_i - \sum_{j\in C}\sum_{i} W_{ij}' U_j = -\sum_{j\in C}\sum_{i\in R} W_{ij}' U_j \qquad (4.5.31)$$

λ is then estimated by the expression

$$\lambda \cong \frac{\sum_j (S_j - U_j \sum_R W_{ij}')}{\sum_j S_j/k_j} \qquad (4.5.32)$$

Turning to the modified TRILUX equation, it is

$$\sum_v W_{ij}' U_j - \sum_v W_{ji}' U_i + \lambda S_j/k_j - S_j + \sum W_{ij}'(1-\beta)U_j = 0 \qquad (4.5.33)$$

The only change is due to the term $\Sigma W_{ij}'(1-\beta)U_j$, and the modified estimate for λ becomes

$$\lambda \cong \frac{\sum_j (S_j + \sum_i W_{ij}'(1-\beta)U_j - U_j \sum_R W_{ij}')}{\sum_j S_j/k_j} \qquad (4.5.34)$$

4.5.2. Results of calculating axial cell power distribution

The axial cell power shapes fall into three categories: First, a cell may be uncontrolled, i.e. no control rods are inserted. In that case the power distribution will be peaked in the lower half of the cell. This is due to the existence of voids which increase monotonically from bottom to top in the coolant. Second, a control rod may be partially inserted in the cell. If it is inserted midway in the cell, its effect becomes largest on the axial power shape, where the lower part is cut off due to absorp-

tion of the control rod and the upper part with no absorbing material is strongly peaked. Third, a control rod may be inserted fully or nearly so in the cell. In this case the axial power shape becomes similar to that in the uncontrolled cell. The reason for this is that a completely inserted control rod has a uniform effect on the axial power distribution, so that the axial void distribution is the only factor that comes into play.

The axial power distributions of the monitored cells as estimated by the present method have been compared to that calculated by the three-dimensional nodal theory calculation. The axial power shapes are shown in Fig. 4.5.1 - 6 and the corresponding curves for the reflection coefficient are shown in Fig. 4.5.7 - 9. Both the estimated and three-dimensional solutions for the axial cell power shape are drawn with a dotted and full line, respectively.

The axial power shape of the cell consisting of channels 92, 93, 101, and 102 is shown in Fig. 4.5.1. The cell has one control rod inserted 7% ~ 1.75 nodes. The small insertion of the control rod means that the axial power shape is almost like that of an uncontrolled cell. The standard deviation of the per cent error is 2.1%. The reflection coefficient displayed in Fig. 4.5.7 is slightly different from 1. It is slightly greater than 1 for the first four nodes and falls from 0.998 in node 5 to 0.988 in node 16; it remains greater than 1 for the rest of the nodes. The reflection coefficient is greater than 1 or less than 1 depending on whether an inflow or outflow of neutrons take place. The dropping of the reflection coefficient below 1 from node 5 to 15 is caused by the insertion of a control rod through 14 nodes in the neighbour cell consisting of channels 71, 72, 82, and 83; this causes neutrons to leak out of the cell question.

The cell consisting of channels 88, 89, 97, and 98 has one control rod inserted 20% ~ 5 nodes. The axial power shape of this cell is also peaked in the lower half of the cell as seen in Fig. 4.5.2. The standard deviation of the per cent error is 2.3%. The corresponding reflection coefficient is displayed in Fig. 4.5.7. It starts with the value 1.04 in node 1 and decreases, dropping below 1 in node 8, where it is 0.997. In node 11 it at-

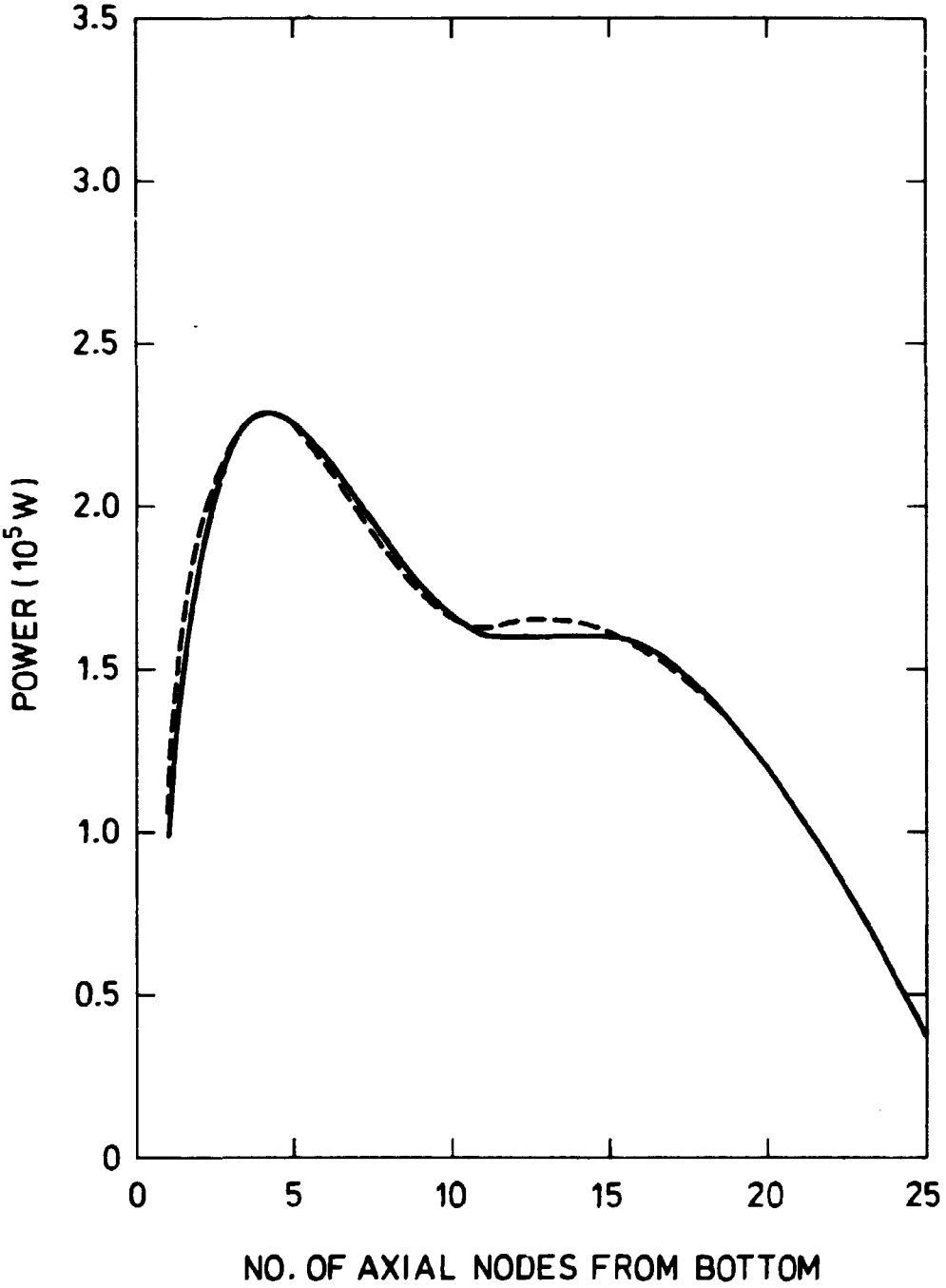

Fig. 4.5.1. Average power shape channels 92, 93, 101, and 102.

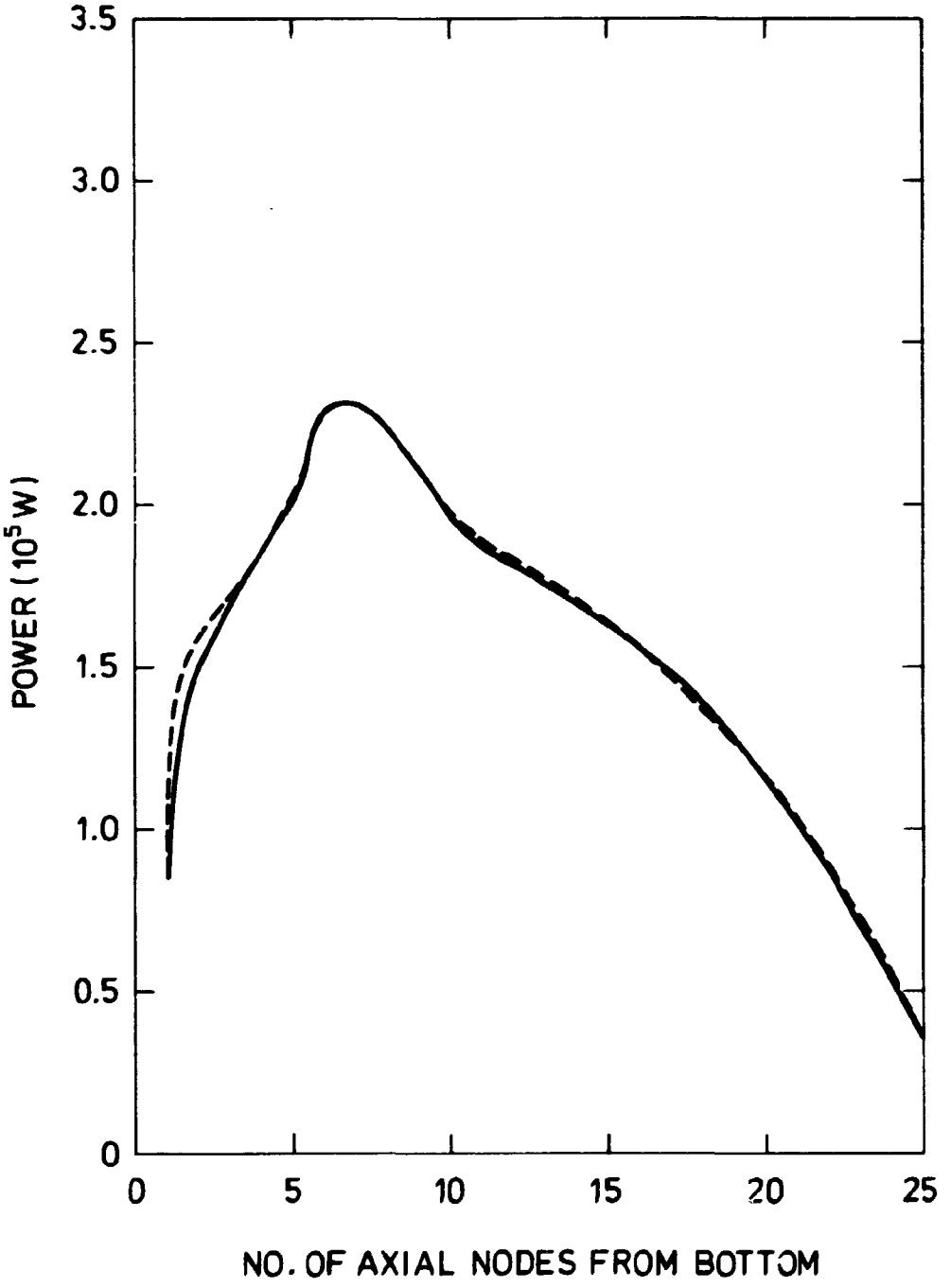

Fig. 4.5.2. Average power shape channels 88, 89, 97, and 98.

tains the minimum value 0.984 and thereafter increases slowly, first becoming greater than 1 in node 23. This behaviour can be explained by the presence of a control rod inserted 24 nodes in the neighbouring cell consisting of channels 67, 68, 78, and 79. With regard to the bottom of the cell the presence of the control rod will make neutrons leak into the cell, which explains why the reflection coefficient becomes greater than one.

The cell consisting of channels 49, 50, 60, and 61 has two control rods inserted in it, one 14% ~ 3.5 nodes and the other is inserted 54% ~ 13.5 nodes. This is thus an example of a case where the control rod is inserted midway. The axial power shape can be decomposed into two components: the unperturbed shape corresponding to the shallow control rod and a shape strongly peaked in the upper half of the core. The axial power shape is shown in Fig. 4.5.3. The standard deviation of the per cent error is 5.0%. The reflection coefficient is shown in Fig. 4.5.8. It starts with the value 1.049 and decreases until it falls below 1 in node 14, remaining there for the rest of the nodes. It is greater than 1 until node 13 due to the control rod which is inserted 54% and drops below 1 thereafter because of the control rod in the cell consisting of channels 47, 48, 58, and 59 which is inserted 96% and the control rod in the cell consisting of channels 27, 28, 38, and 39 which is inserted 87%.

The cell consisting of channels 1, 2, 12, and 13 has two control rods inserted. One of them is inserted 22% ~ 5.5 nodes and the other is inserted 61% ~ 15.3 nodes. The axial power shape is shown in Fig. 4.5.4. The standard deviation of the per cent error is 2.7%. It is strongly peaked in the upper half of the core. The reflection coefficient is shown in Fig. 4.5.8. It starts in node 1 with the value 1.063, drops to 1.007 in node 16, and thereafter remains close to 1. Two of the neighbour cells have only one control rod inserted 61% and therefore some inflow of neutrons will take place at the bottom.

The cell consisting of channels 45, 46, 56, and 57 has one control rod inserted 96% ~ 24 nodes. The axial power shape is shown in Fig. 4.5.5. The standard deviation of the per cent error is

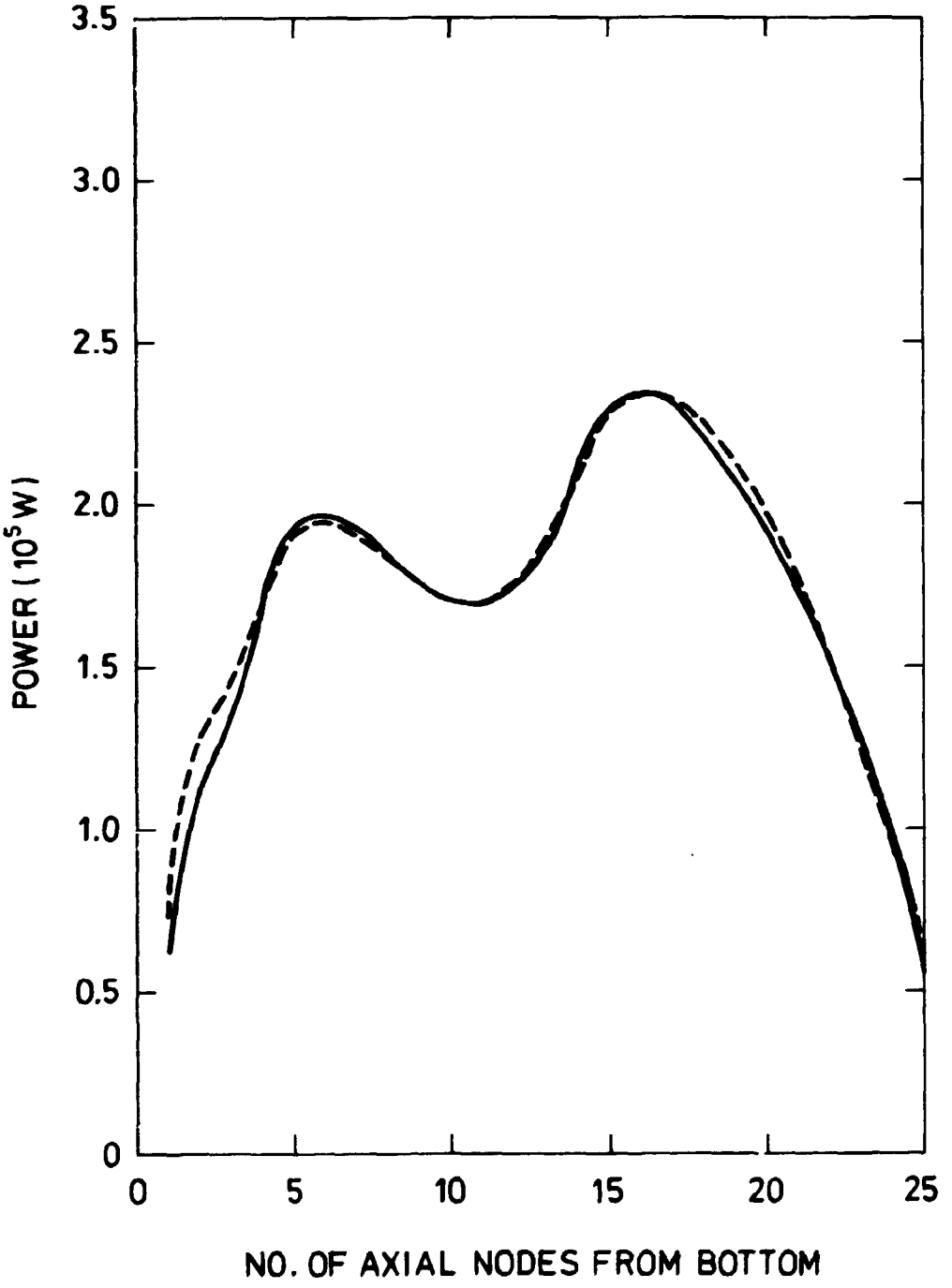

Fig. 4.5.3. Average power shape channels 49, 50, 60, and 61.

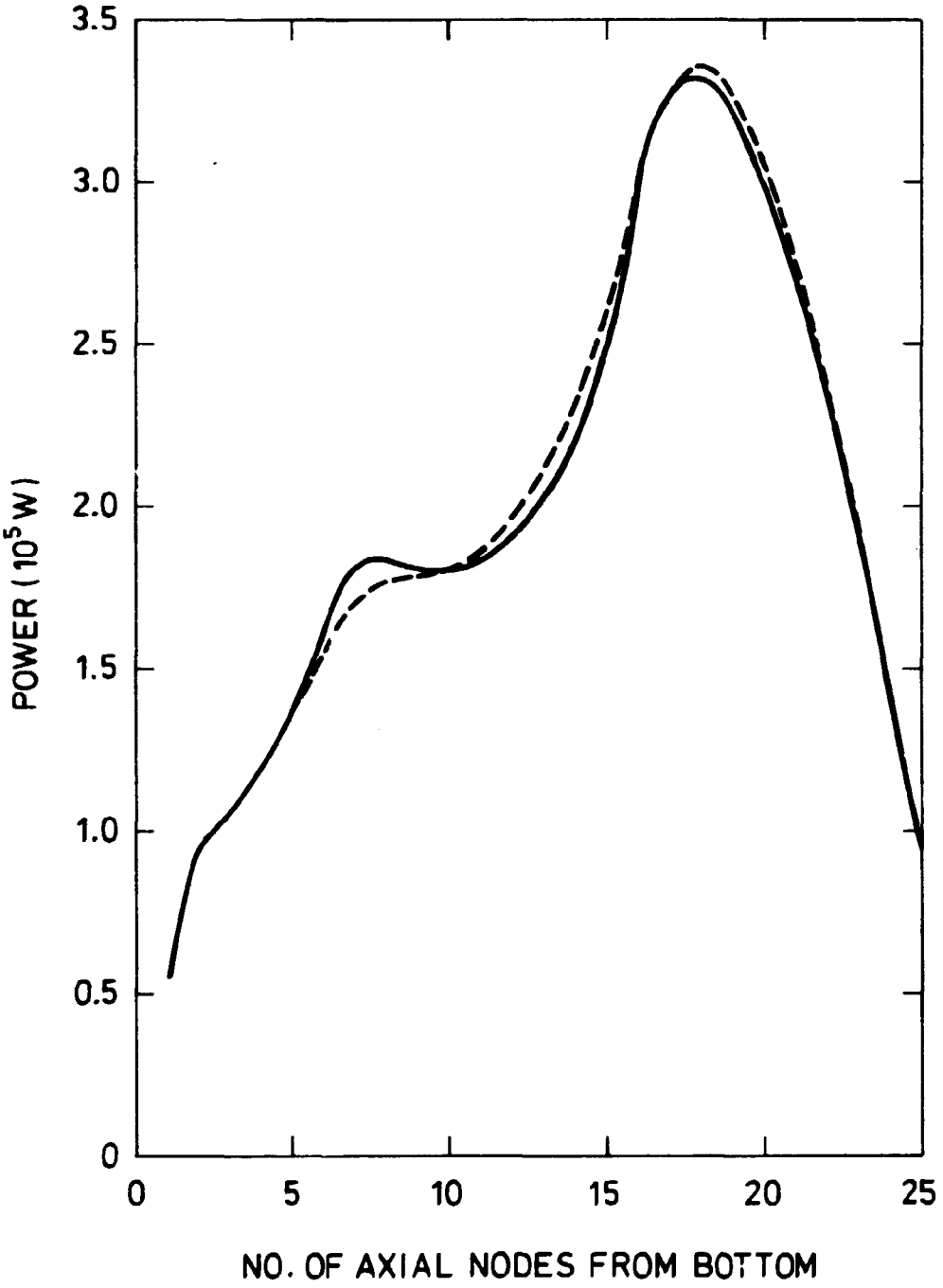

Fig. 4.5.4. Average power shape channels 1, 2, 12, and 13.

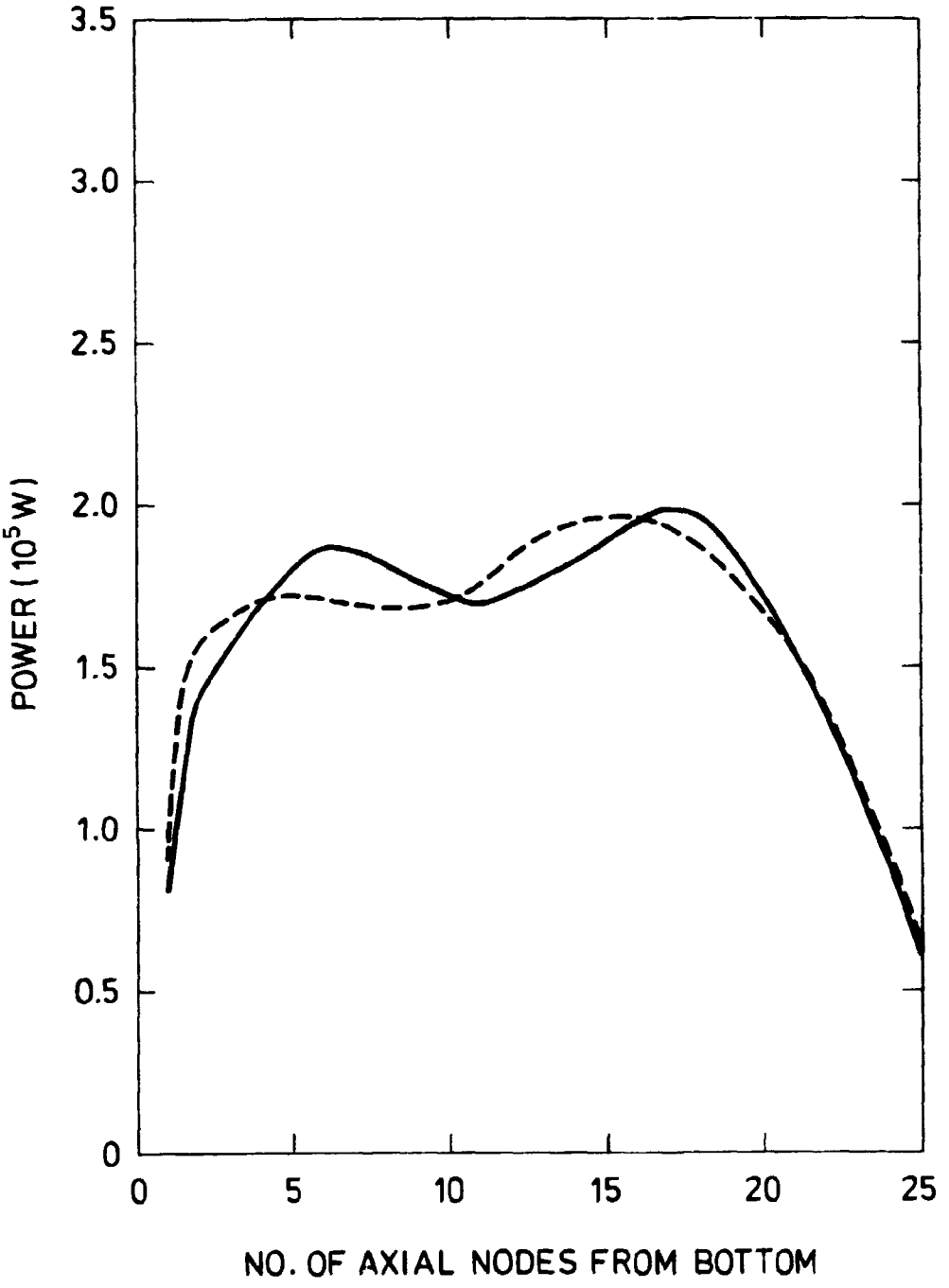

Fig. 4.5.5. Average power shape channels 45, 46, 56, and 57.

5.9%. Since the control rod is nearly fully inserted, it should be peaked in the lower half of the core. Instead a peak occurs both in the upper and the lower part of the core, the distribution being rather flat. This is due to the neighbouring cell consisting of channels 23, 24, 34, and 35 which has a control rod inserted 61% ~ 15.3 nodes. Turning to the reflection coefficient shown in Fig. 4.5.9, it starts with the value 0.961 in node 1, is nearly constant to node 4, where it is 0.968, grows to 0.995 in node 10, then to 1.021 in node 16, to 1.037 in node 22, and is nearly constant for the rest of the nodes. Clearly, control rods of neighbouring cells account for the leakage out in the lower half, whereas an inflow takes place in the upper half because of the absence of a control rod in the cell consisting of channels 23, 24, 34, and 35. A similar behaviour is displayed by the cell consisting of channels 5, 6, 16, and 17, the power shape of which is shown in Fig. 4.5.6 with corresponding reflection coefficient in Fig. 4.5.9. The standard deviation of the per cent error is 6.3%.

The estimated power shapes seem in agreement with the reference power shapes in Fig. 4.5.1-4, but in Fig. 4.5.5-6 the deviation is rather great. A possible explanation is that the power shapes of Fig. 4.5.5-6 are strongly influenced by control rods outside the cell, whereas the power shapes of Figs. 4.5.1-4 are determined principally by control rods inside the cell, and these are used directly in the calculations.

Figure 4.5.10 shows the radial cell power distribution for monitored cells, and Fig. 4.5.11 that for unmonitored cells.

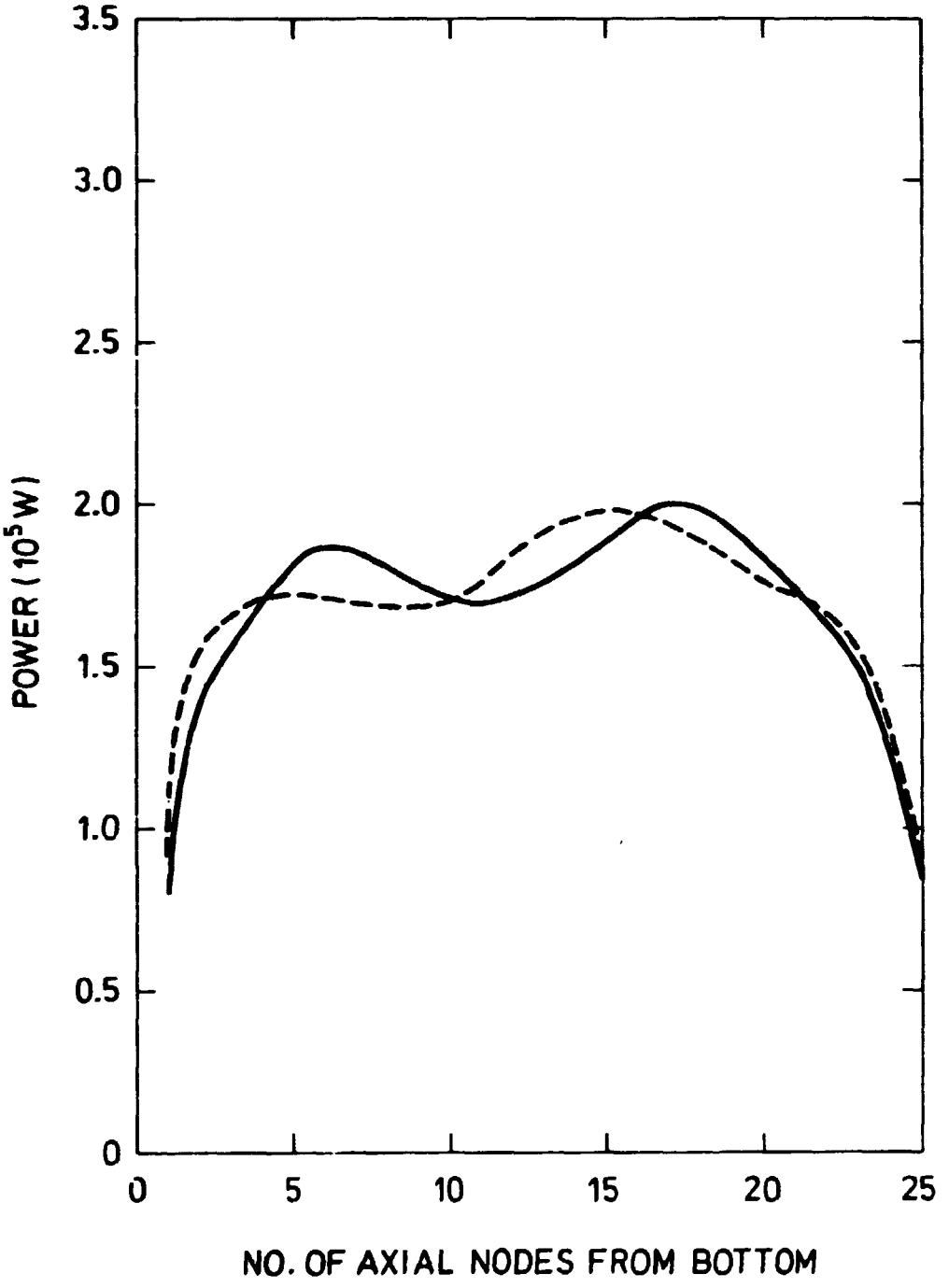

Fig. 4.5.6. Average power shape channels 5, 6, 16, and 17.

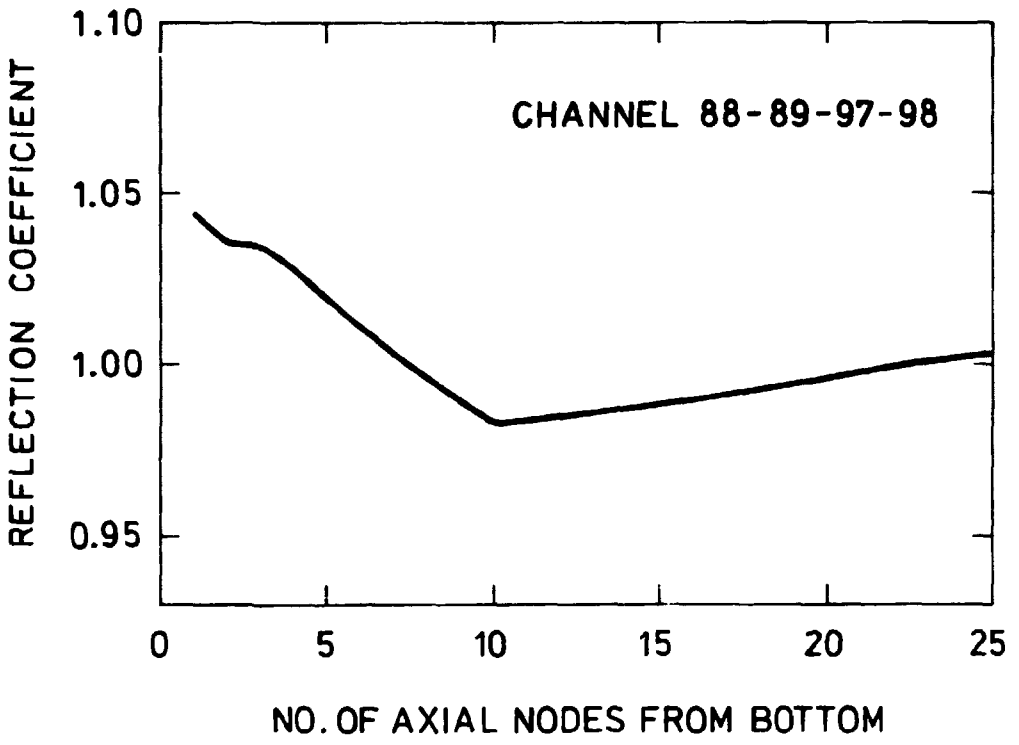

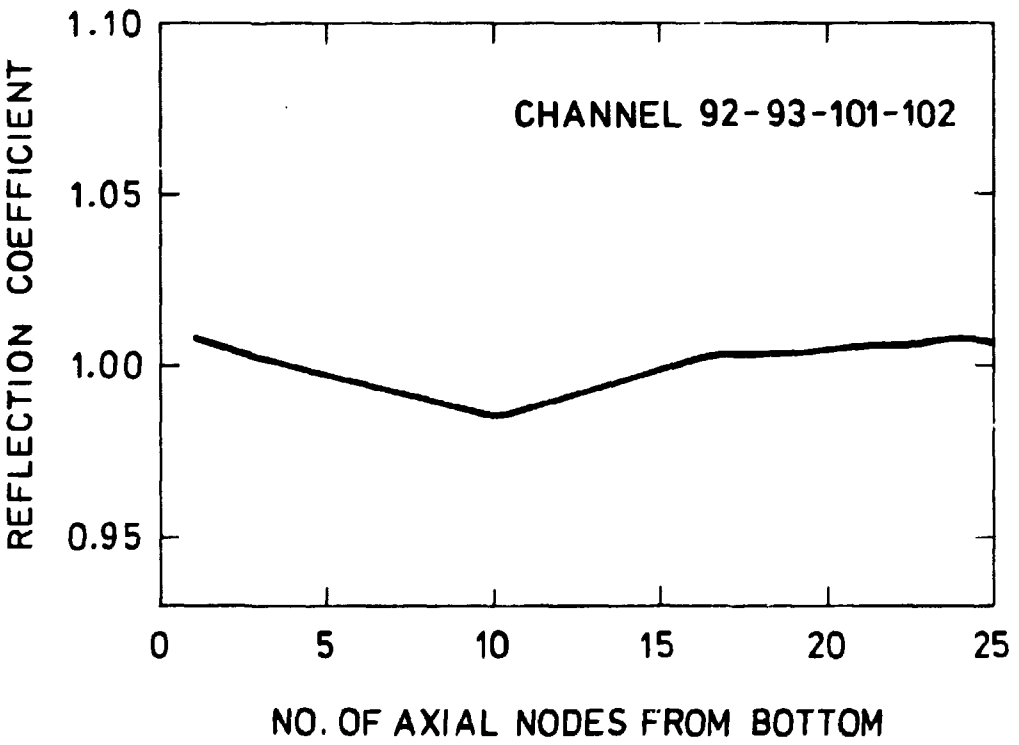

Fig. 4.5.7. Reflection coefficient versus axial node level.

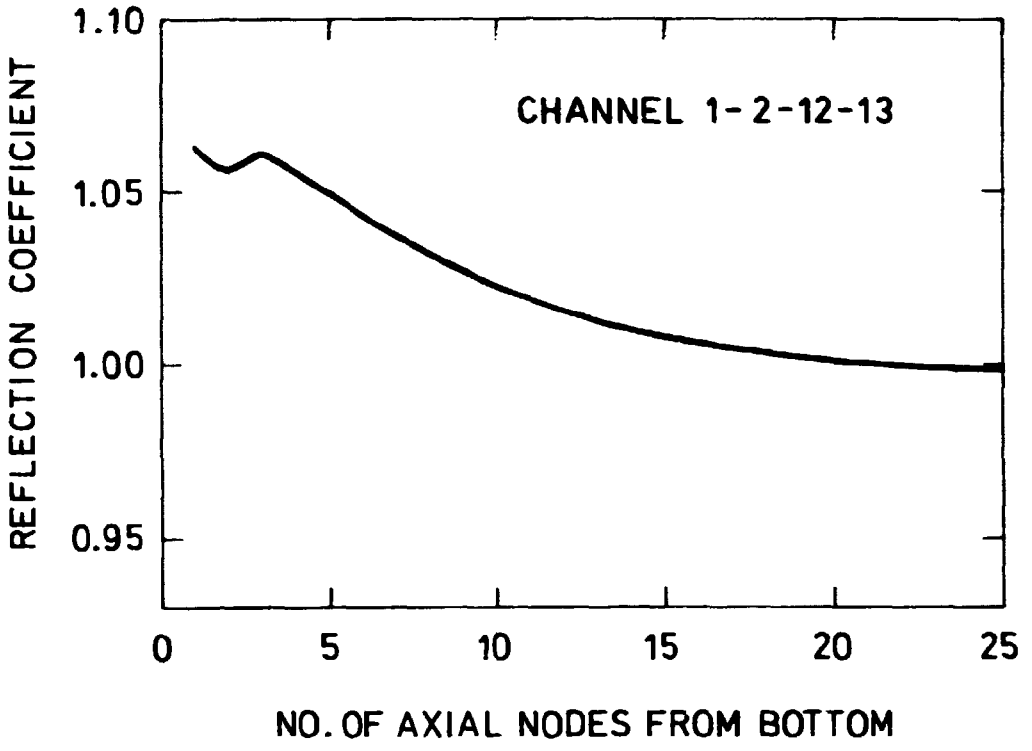

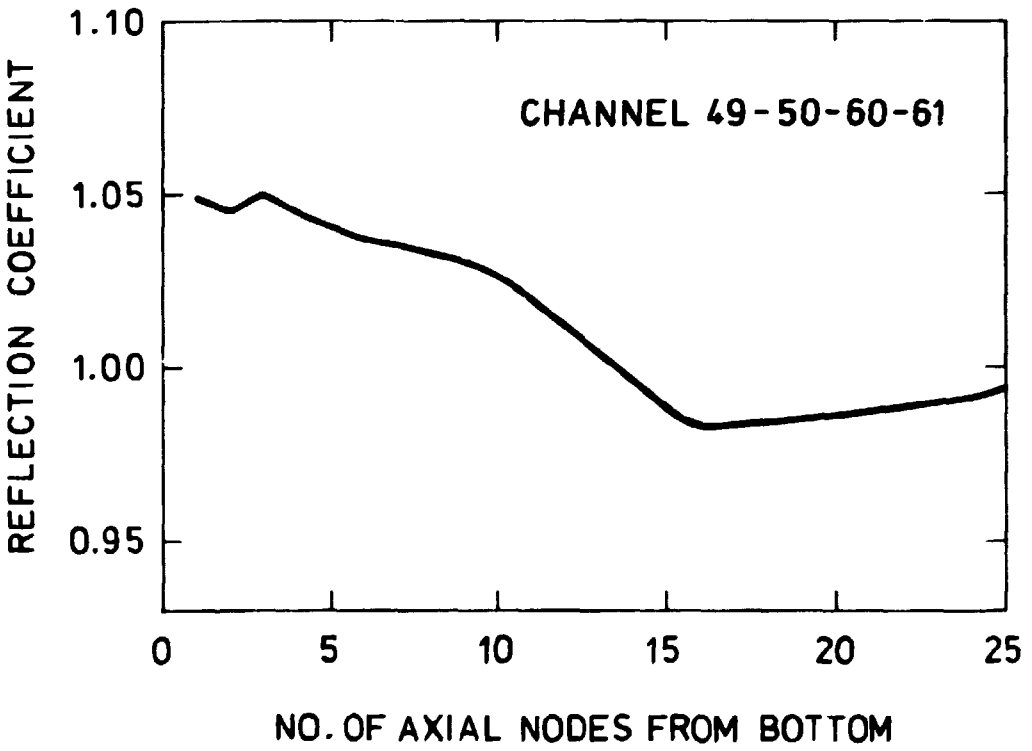

Fig. 4.5.8. Reflection coefficient versus axial node level.

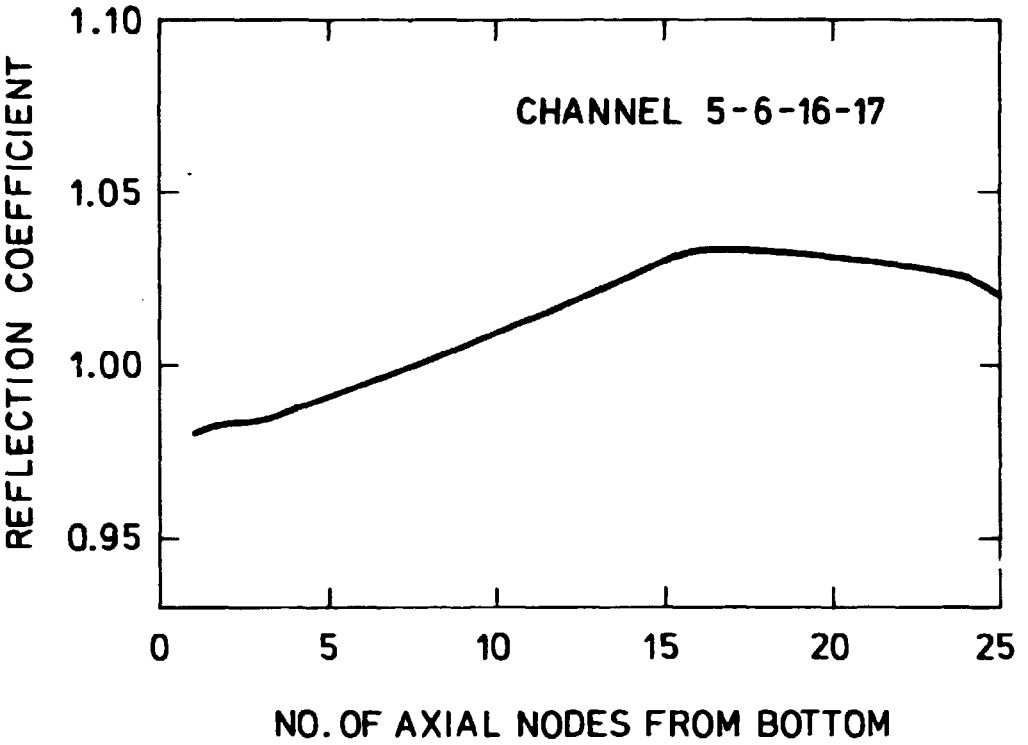

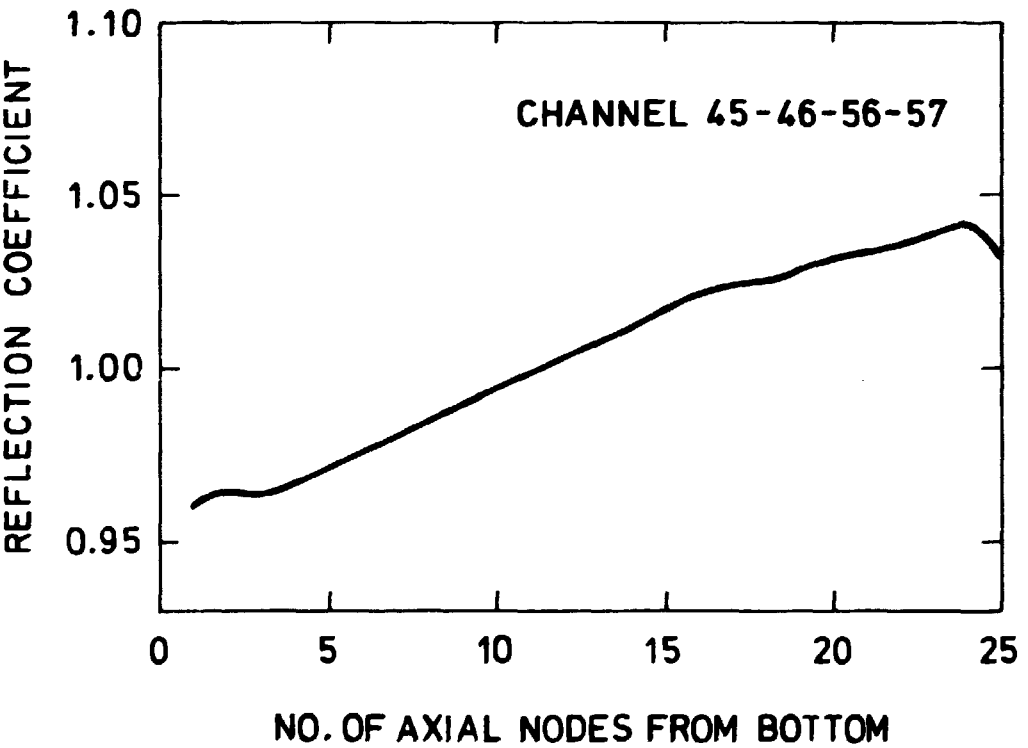

Fig. 4.5.9. Reflection coefficient versus axial node level.

1.295 1.300		1.095 1.095		1.015 1.020
1.048 1.051		1.115 1.121		0.993 0.996
0.985 0.994		0.983 0.986		

1. FIGURE: REFERENCE CELL POWER
2. FIGURE: ESTIMATED CELL POWER

Fig. 4.5.10. Radial cell power distirbution for monitored cells.

	1.250 1.293		0.998 0.936	
1.235 1.274	1.188 1.215	1.078 1.079	1.030 1.025	1.023 1.085
	1.045 1.043		1.083 1.074	
0.953 0.884	0.993 0.978	1.073 1.059	1.000 0.952	0.798 0.762
	1.013 1.056		0.793 0.759	

1. FIGURE: REFERENCE CELL POWER
2. FIGURE: ESTIMATED CELL POWER

Fig. 4.5.11. Radial cell power distribution for unmonitored cells.

4.6.1 Method for calculating axial box power distribution

Having determined the axial cell power distribution, the power distribution of the boxes of the cell is to be calculated next. Starting in the upper left corner of the cell and moving clockwise round the cell the boxes are given numbers from 1 to 4. The fraction of the cell power produced by a box depends on the presence of control rods and the exposure and void fraction of the box. If a control rod is inserted the fraction is reduced, but on the other hand this makes the void content less than the average of the cell, affecting the fraction in the opposite direction. A greater exposure than the cell's average exposure similarly means that less power is to allocated to the box in question. The void content and exposure of a box can be regarded as perturbations of the average void content and exposure of the cell, leaving the control rod configuration as the dominant parameter. Let I denote the index of a box in a cell and K the number of axial nodes from the bottom, and let C denote the control rod pattern. The control rod pattern is characterized by either no control rods per cell, one rod, or two. Then f(I,K,C) is defined as the power of box I divided by the total cell power at axial level K with control rod pattern C. f(I,K,C) is determined using a box calculation (diffusion theory in two dimensions) in which the four boxes of the cell are represented. The calculation is performed for no control rods per cell, one, and two per cell. A void content of 0% and reflecting boundary conditions were assumed. A calculation made at a void content of 75% showed that the change in f(I,K,C) was negligible, and so only results corresponding to a void of 0% were used. The assumption of reflecting boundary conditions will, however, introduce an error, since conditions change from cell to cell in the reactor. If a box is adjacent to one in a neighbour cell with higher power, the former's power will be raised compared to the power predicted by the correlation factor f(I,K,C).

A way to overcome this difficulty is to use the results from the calculation of the estimated detector readings of cells without instrumentation. Let the power of a cell at an axial level K be $P_{CELL}(K)$, and let the power of box I belonging to

the cell be $P_{BOX}(I,K)$ as determined by the two-dimensional detector reading calculations. At each detector level a radial leakage correction factor can now be obtained as

$$RLEAK(I,K) = P_{BOX}(I,K)/(P_{CELL}(I,K,C)) \qquad (4.6.1)$$

Between the detector levels the correlation factor is determined by linear interpolation of the values of the detector levels. The correlation factors are generated presuming the same void content for all the boxes of the cell. When a control rod is adjacent to a box, the power of that box is reduced, and the void content becomes greater than that of the other boxes. To take the increased moderation into account a void correction factor CVM(I,K) is introduced. A typical reduction of the void content caused by the presence of a control rod is 10%. This value is assumed for all controlled boxes. A change by 10% will have an effect depending on the average void fraction of the cell. Thus a greater effect is expected at higher average void fractions. From a two-dimensional diffusion theory calculation on four boxes with one control rod inserted the relative change of the power of the boxes caused by a reduction of the void content of the controlled boxes by 10% were found to be

void content	controlled box	adjacent box	opposite box diagonally
10%	0.046	- 0.007	- 0.012
40%	0.061	- 0.009	- 0.016
60%	0.077	- 0.011	- 0.021
70%	0.087	- 0.012	- 0.024

The void contents used are the average void fractions of detector level A, B, C, and D. Between the detector levels the correction factor is found by linear interpolation. Now an overall correction factor CR(I,K) can be determined as

$$CR(I,K) = CVM(I,K) + RLEAK(I,K) \qquad (4.6.2)$$

and the box power calculated by using correlation factors is multiplied by this factor to get an improved estimate.

4.6.2. Results of calculating axial box power distribution

The correlation factors used for the calculation of the axial box power distribution are shown in Fig. 4.6.1. The factors are given for the case with one and two control rods inserted. The factors are normalized so that their sum is equal to unity. If one control rod is inserted, the box nearest it experiences a decrease in power by 31.1% relative to the average power of the boxes of the cell. The power increases by 7.6% in both of the adjacent boxes and by 16.1% in the diagonally opposite box. If two control rods are inserted the boxes nearest them experience a decrease in power by 19.2%, and the boxes adjacent to them have an increase by the same amount.

The cell consisting of channels 49, 50, 60, and 61 is monitored. Axial power shapes of boxes of that cell are shown in Fig. 4.6.2-4. The shapes drawn with full line are determined by the three-dimensional nodal calculation, and those drawn with dotted line are estimated by the present method. The cell has two control rods inserted, one by 14% ~ 3.5 nodes, and one by 54% ~ 13.5 nodes. The bundle power distribution is shown in Fig. 4.6.6. In this way the three-dimensional power distribution is estimated within 14% of a three-dimensional nodal theory calculation. The three-dimensional nodal theory calculation lasts for 2220 s in CPU-time, while a calculation by the present method lasts for 450 s in CPU-time.

To examine the influence of the void content on the correlation factor a two-dimensional diffusion theory calculation on a cell of four boxes has been made for all void fractions in the interval from 0% to 70%. The cell was uncontrolled. At each cell void fraction the void fraction of box 1 in Fig. 4.6.5 was raised 10%. This is a typical change caused by the presence of a control rod. The relative change of the power level for the various boxes was calculated. Fig. 4.6.5 shows the results. For box 1 the power change increased from -3.3% at 0% void to -7.4% at 70% void. For box 2 it increased from 1.0% at 0% void to 2.0% at 70% void. For box 3 it increased from 1.4% at 0% void to 3.4% at 70% void. Increasing the average void content attaches more importance to a change of the void content of a given amount.

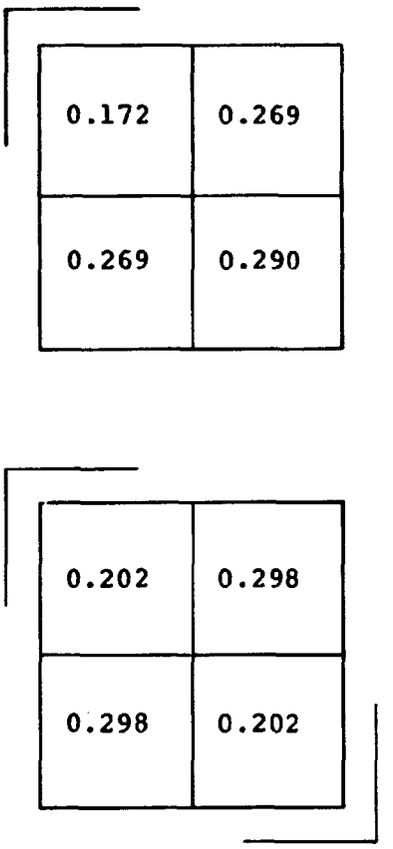

Fig. 4.6.1. Correlation factors for cells with one and two control rods inserted.

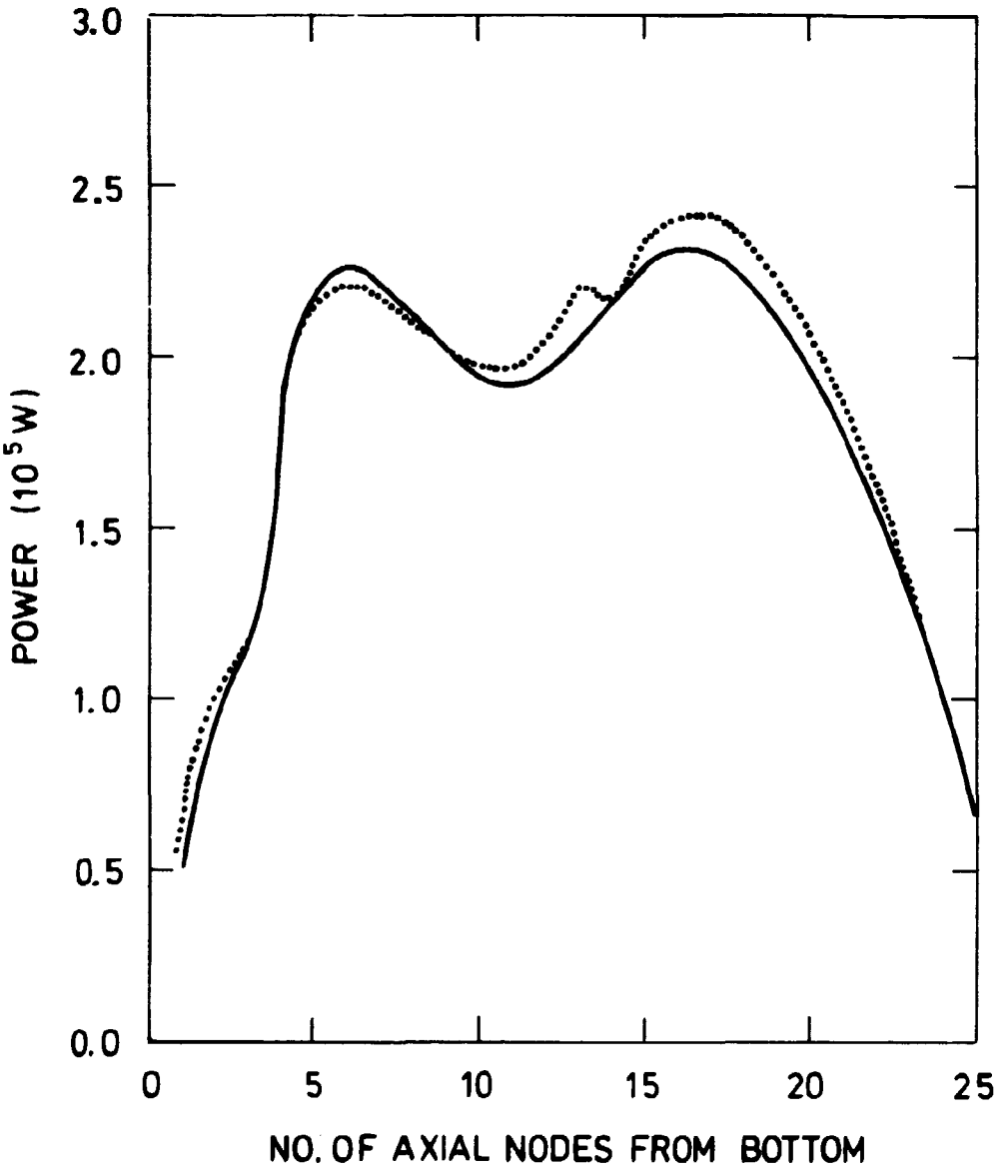

Fig. 4.6.2. Axial box power shape of channel 49.

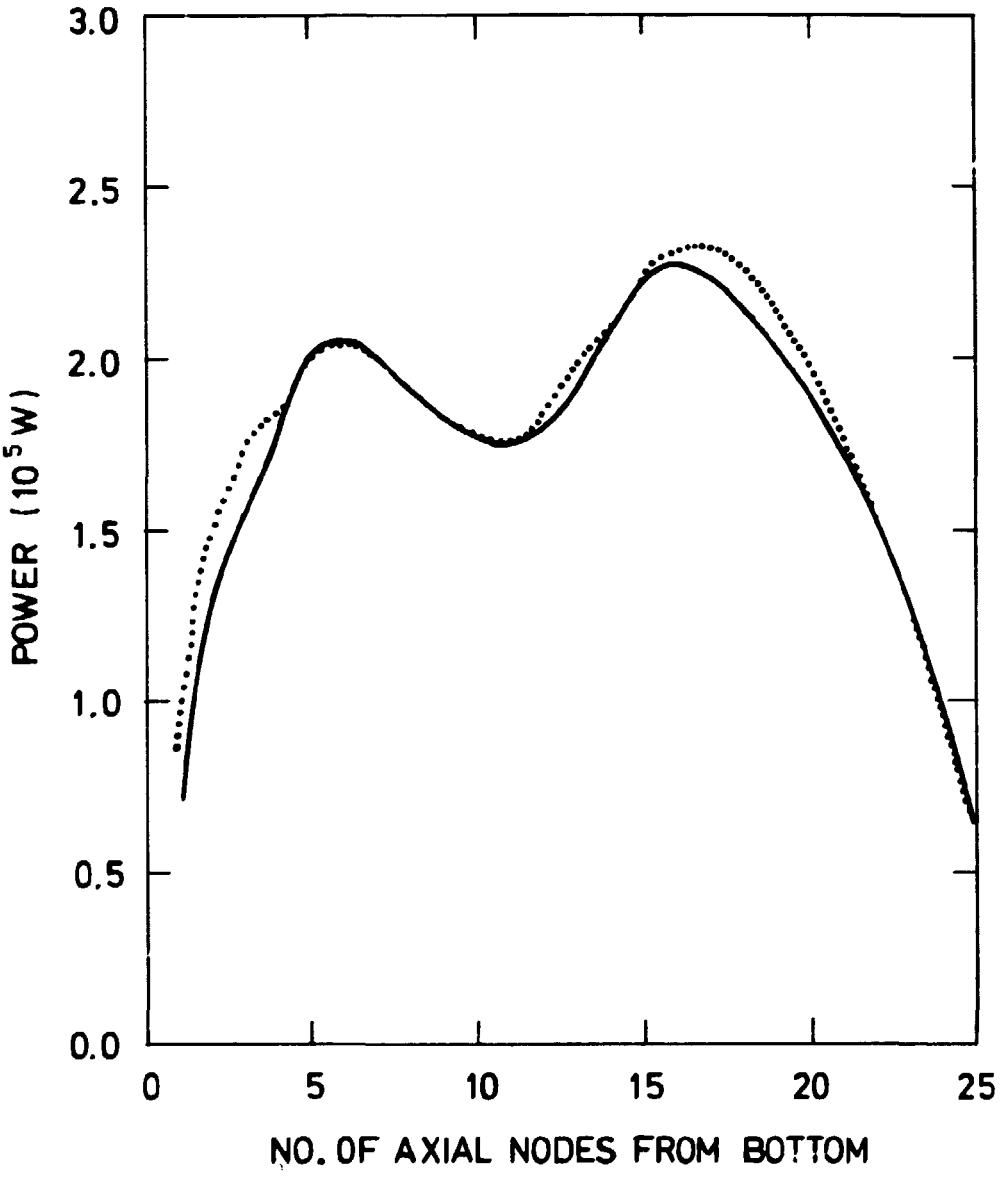

Fig. 4.6.3. Axial box power shape of channel 50.

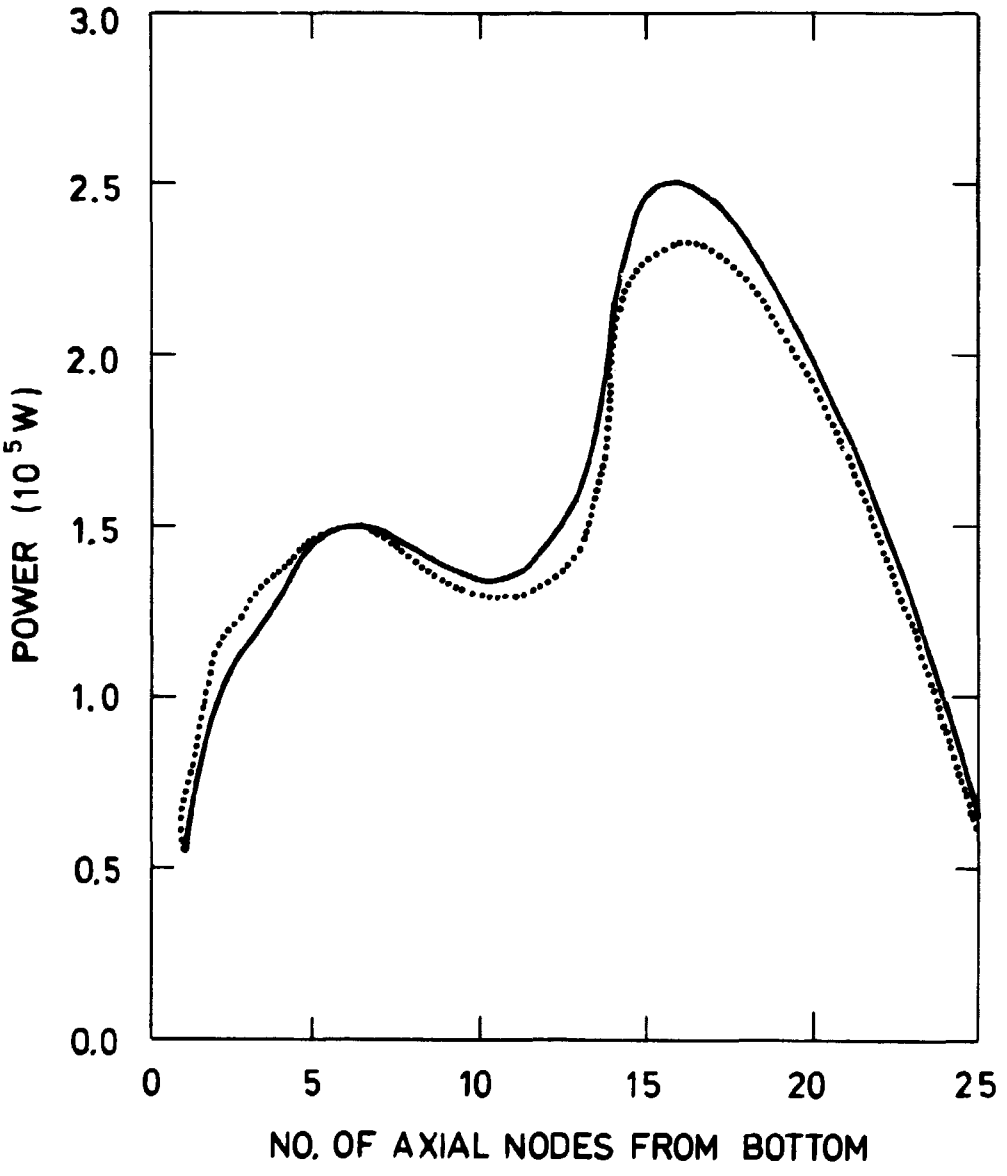

Fig. 4.6.4. Axial box power shape of channel 61.

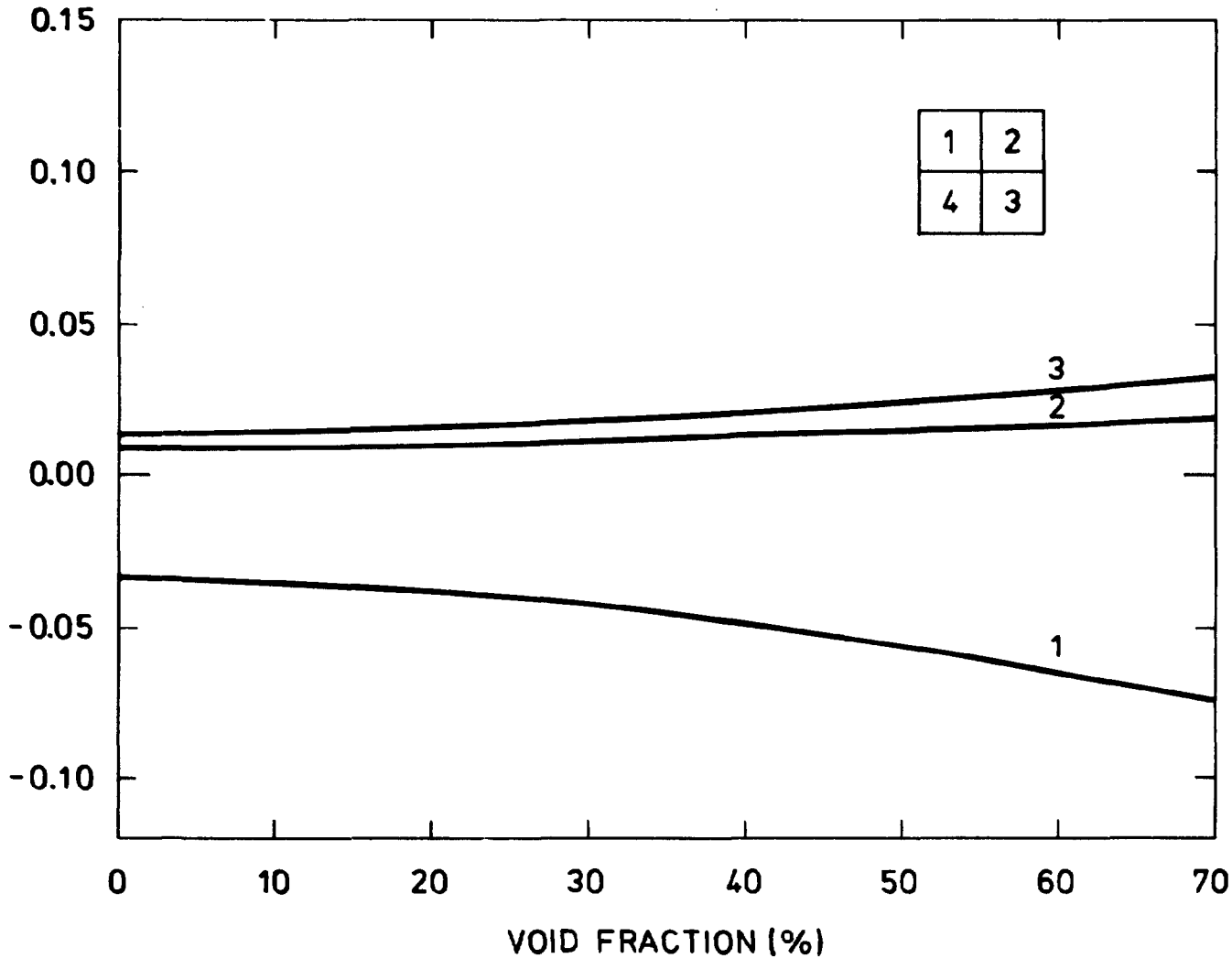

Fig. 4.6.5. Relative change of box power versus void fraction.

1.35	1.32	1.30	1.30	1.23	1.10	1.04	1.06	1.06	0.96
1.36	1.35	1.35	1.38	1.28	1.08	0.98	0.98	1.02	0.97
1.32	1.19	1.16	1.24	1.16	0.89	0.85	1.04	1.08	0.96
1.34	1.15	1.15	1.29	1.18	0.85	0.78	1.00	1.08	1.01
1.29	1.15	1.13	1.21	1.14	0.89	0.86	1.06	1.09	0.94
1.34	1.14	1.12	1.26	1.16	0.86	0.82	1.05	1.13	1.03
1.28	1.22	1.20	1.21	1.18	1.10	1.08	1.12	1.10	0.96
1.36	1.27	1.24	1.25	1.19	1.12	1.09	1.14	1.14	1.03
1.19	1.12	1.11	1.16	1.17	1.14	1.12	1.13	1.09	0.94
1.24	1.14	1.12	1.17	1.20	1.16	1.13	1.14	1.10	0.97
1.05	0.83	0.83	1.08	1.13	1.02	1.00	1.08	1.05	0.89
1.03	0.80	0.81	1.08	1.15	0.99	0.95	1.07	1.03	0.88
1.00	0.79	0.80	1.05	1.10	1.00	0.97	1.03	0.97	0.79
0.93	0.73	0.77	1.05	1.11	0.94	0.90	1.00	0.94	0.76
1.02	1.00	1.03	1.09	1.11	1.08	1.03	0.97	0.81	0.62
0.94	0.95	1.00	1.10	1.12	1.06	0.99	0.92	0.78	0.58
1.02	1.05	1.07	1.08	1.08	1.04	0.96	0.81		
1.00	1.05	1.09	1.12	1.08	1.03	0.93	0.78		
0.93	0.94	0.95	0.95	0.93	0.88	0.78	0.62		
0.94	0.99	1.01	1.01	0.96	0.87	0.75	0.57		

1. FIGURE: REFERENCE BUNDLE POWER
2. FIGURE: ESTIMATED BUNDLE POWER

Fig. 4.6.6. **Radial bundle power distribution.**

5. DETECTOR CONSTANTS

5.1. Parametric study of detector constants

Until now the detector readings have been assumed to be proportional to the average power density. Some calculations have been performed in order to investigate the influence of various parameters on the detector readings. The detector readings are now assumed to be proportional to the average power of the four fuel rods immediately surrounding the detector. The calculations are made using CDB[13], a fuel box burnup program using a collision probability method for calculating flux in the pin cells and diffusion theory for the flux calculation in the fuel box. In all calculations ten energy groups, six of which are in the thermal region, are used. In the diffusion calculation five groups are used. The cross sections are generated on the basis of a pin with an enrichment equal to the average of that of the pins and with a surrounding water layer to take the influence of the water gaps into account.

Parameters of particular interest are the void fraction and the control rods. Calculations have been performed for four boxes without control rods, with one control rod, and with two control rods varying the void fraction from 0% to 75%. The relative TIP-reading defined as the ratio of the average rod power at the actual void fraction to that at 0% void is shown in Fig. 5.1.1-3. From these curves it appears that changing the void fraction from 0% to 75% decreases the relative TIP reading by 12% for an uncontrolled cell, by 11% for a cell with one control rod, and by 10.5% for a cell with two. If the average pin power of the cell is 1000, the average power of the corner rods at 0% void will be 1034 for an uncontrolled cell, 1101 for a cell with one control rod, and 1212 for a cell with two. Thus one control rod increases the detector reading by 6.5% and two increase it by 17.2%. A control rod results in a strong flux tilt away from

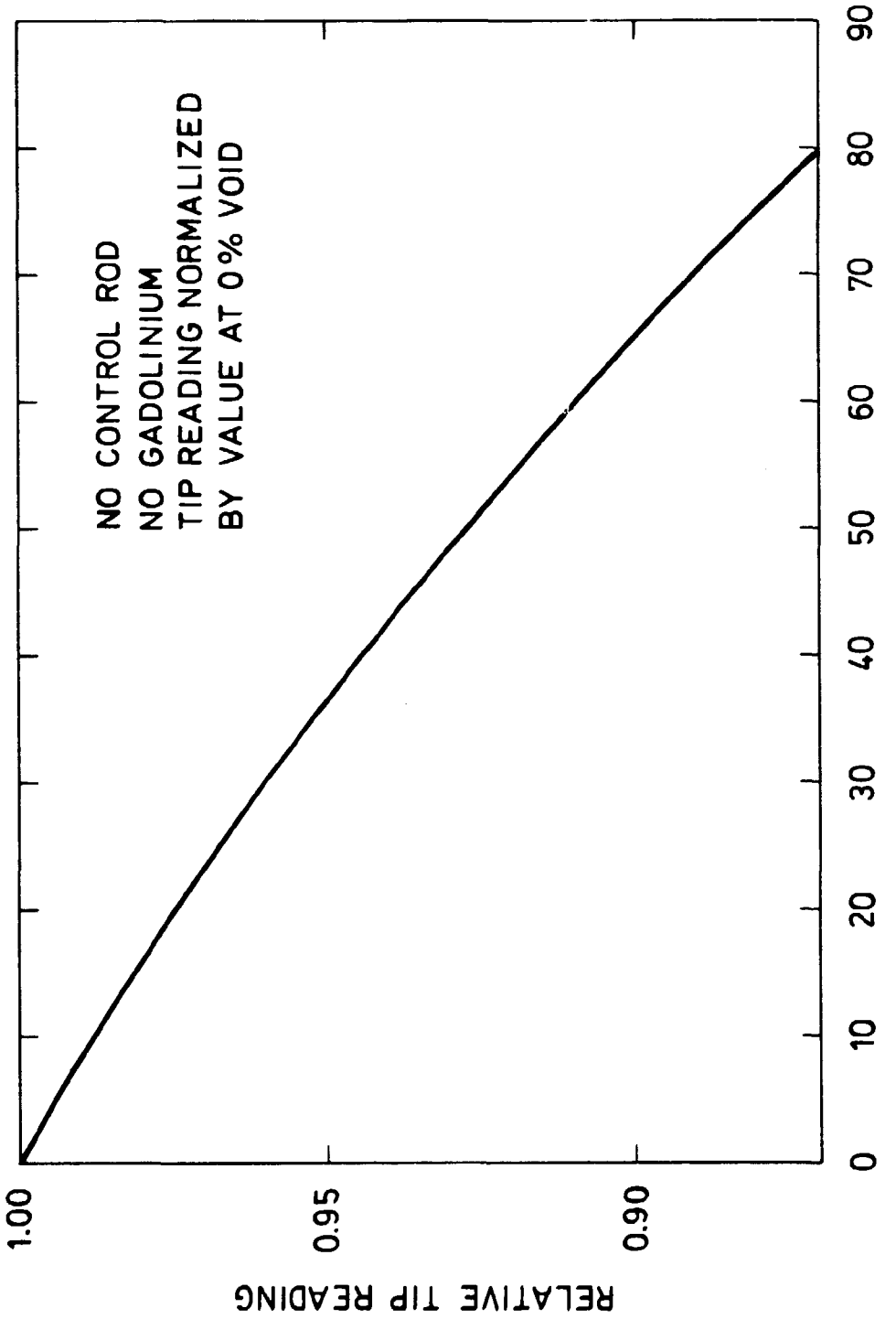

Fig. 5.1.1. Relative TIP-reading versus void fraction.

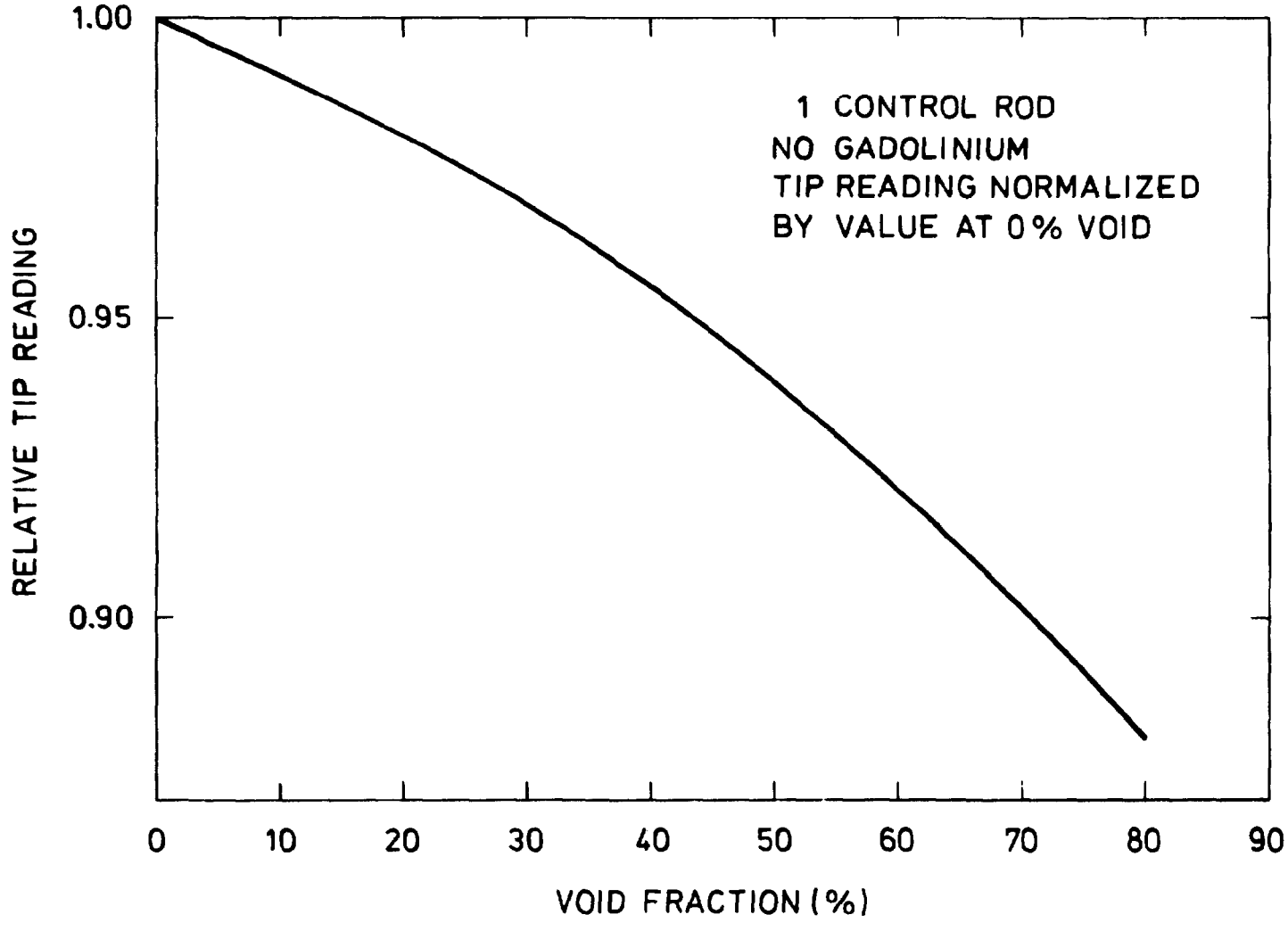

Fig. 5.1.2. Relative TIP-reading versus void fraction.

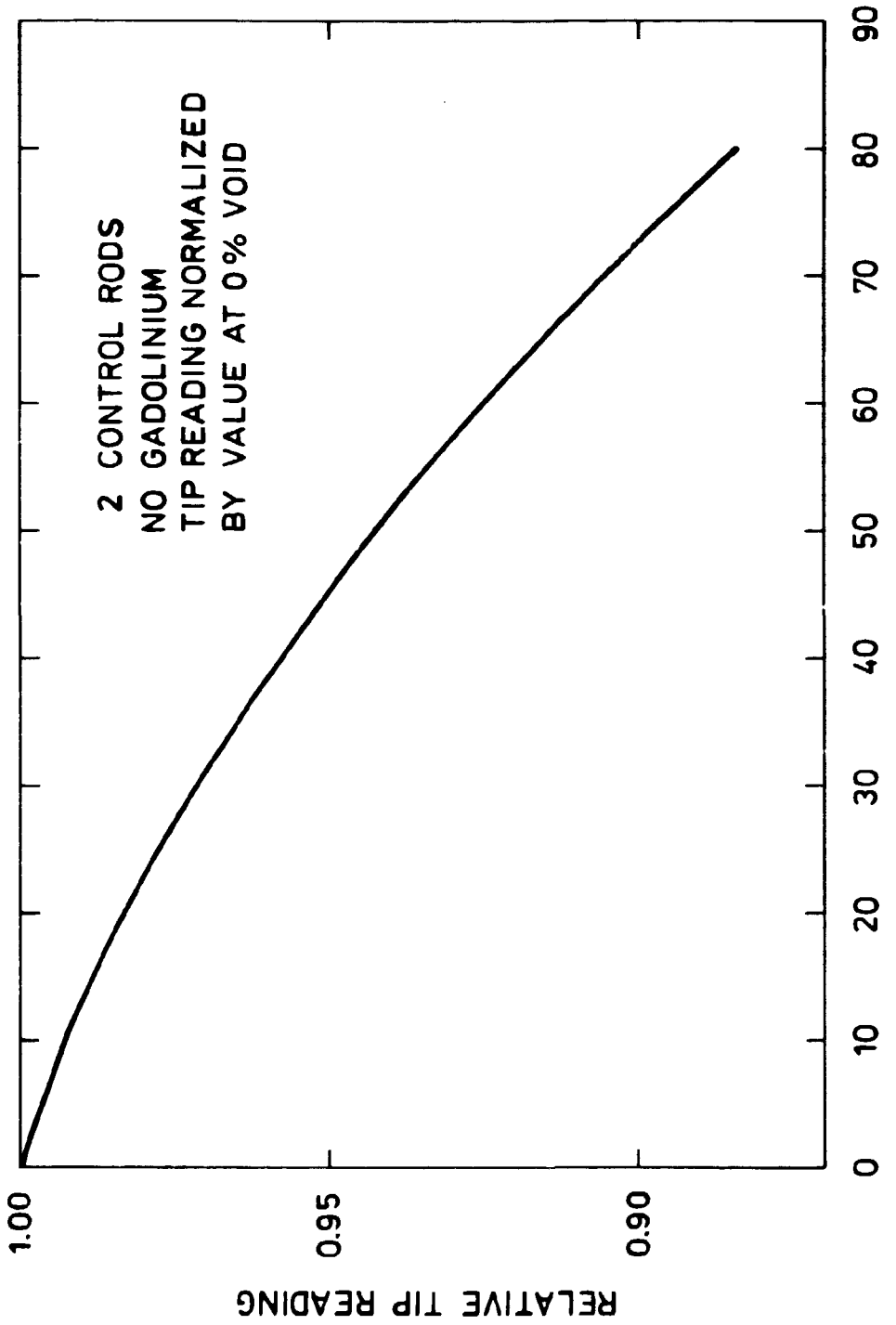

Fig. 5.1.3. Relative TIP-reading versus void fraction.

the controlled corner, thus raising the detector reading. The reason that the detector reading falls with increasing void fraction is that the water gaps around a fuel box have varying widths. Thus the water gaps accomodating the control rod are broader than the water gaps at the detector's location. Raising the void fraction of the boxes, the greater amount of water in the broad water gaps becomes more important as the amount of water within the flow box decreases. The result is an increased power of pins adjacent to the broad water gaps and a decrease in the power of pins adjacent to the narrow ones. As the detector reading is proportional to the power of pins which are adjacent to narrow water gaps, it consequently falls.

5.2. Uncertainties in determinating the detector constants

The detector readings are very sensitive to changes in the surroundings. Thus an inhomogeneous void distribution caused by the presence of a water film inside the flow box may change the detector reading by as much as 10%, if the void fraction is 75% and the thickness of the water film is 1 mm[14]. A similar effect occurs when the water gap width varies due to flow box bowing.

6. CONCLUSION

A calculational procedure has been set up for estimating three-dimensional power distributions in a boiling-water reactor core using in-core detector readings. The reactor is grouped in cells, each of which consists of four fuel boxes surrounding a detector string, along which neutron detectors are situated. First, the detector readings are calculated that would have been measured in the cells without detectors, if they were instrumented. This calculation is performed in two dimensions at each detector level and is accelerated by means of the readings of the detectors at that level. Second, the axial cell power dis-

tribution is calculated by performing a one-dimensional calculation for each cell in the reactor; this is forced to produce the readings of the detectors of the cell. Third, the axial box power distribution is determined by multiplying the axial cell power by correlation factors. Calculations on a quarter core of a boiling-water reactor have demonstrated the suitability of the calculational procedure for core surveillance systems. Combining one-dimensional calculations on cells and two-dimensional calculations at the detector levels with correlation factors makes the computing time much less than a whole-core three-dimensional nodal theory calculation. On the other hand, the application of these simple methods will lead to reduced accuracy, and this must be taken into account when using them.

REFERENCES

1) FISHER, J.R. (1977). Review of in-core power distribution measurements: Technical Status and Problems. EPRI-NP-337, 201 pp.
2) SCHRÜFER, E. et al. (1974). Strahlung and Strahlungsmesstechnik in Kernkraftwerken. (Elitera, Berlin) 448 pp.
3) CAREW, J.F. (1974). Process computer performance evaluation accuracy. NEDO-20340, 64 pp.
4) HENRY, A.F. (1972). Refinements in accuracy of coarse-mesh finite-difference solution of the group-diffusion equations. In: Proceedings of an IAEA seminar on numerical reactor calculations, (STI/PUB/307). IAEA-SM-154/21, 447-471.
5) BONALUMI, R., GIORCELLI, M., and VIMERCATI, G. (1976). COMETA: An ultra-coarse mesh, three-dimensional diffusion code. In: Nuclear Energy Maturity, Part 2, Vol. 4. Proceedings European Nuclear Conference. Paris, April 1975. (Pergamon, Oxford) 229-236.
6) BASSANI, A. and BOTTONI, G.P. (1979). Interpretation of in-core measurements by a semianalytical approach. Trans. Am. Nucl. Soc. 31, 250-253.

7) DELP, D.L. et al. (1964). FLARE, A three-dimensional boiling water reactor simulator. GEAP-4598, 95 pp.

8) NISHIZAWA, Y., KIGUCHI, T., and MOTODA, H. (1976). On-line prediction of the power distribution within boiling water reactors. Nucl. Sci. Eng. 60, 189-192

9) KIGUCHI, T. et al. (1978). On-line core performance evaluation and operating guidance system for BWR. In: Proceedings of an International IAEA Symposium on Nuclear Power Plant Control and Instrumentation 1978. (STI/PUB/491), Vol. 1. IAEA-SM-226/30, 449-462.

10) UCHIKAWA, S., and MOTODA, H. (1981). A method for calculating power distributions in boiling water reactors using in-core detector readings. Nucl. Sci. Eng. 77, 137-145.

11) GOLDSTEIN, L. et al. (1967). Calculation of fuel-cycle burnup and power distribution of DRESDEN-1 reactor with the TRILUX fuel management program. Trans. Am. Nucl. Soc. 10, 300.

12) HENRY, A.F. (1959). A theoretical method for determining the worth of control rods. WAPD-218, 56 pp.

13) LINDSTRØM JENSEN, K.E. (1970). Development and verification of nuclear calculation methods for light-water reactors. RISØ-R-235, 161 pp.

14) EDENIUS, M. (1980). Analysis of BWR bundles with nonuniform void within the channel. Trans. Am. Nucl. Soc. 35, 543-544.

Sales distributors:
G.E.C. Gad Strøget
Vimmelskaftet 32
DK-1161 Copenhagen K, Denmark

Available on exchange from:
Risø Library, Risø National Laboratory,
P.O.Box 49, DK-4000 Roskilde, Denmark

ISBN 87-550-0793-7
ISSN 0106-2840